CrossMark

ORIGINAL PAPER

The Capilla del Monte pluton, Sierras de Córdoba, Argentina: the easternmost Early Carboniferous magmatism in the pre-Andean SW Gondwana margin

Juan A. Dahlquist[1] · Robert J. Pankhurst[2] · Carlos W. Rapela[3] · Miguel A. S. Basei[4] ·
Pablo H. Alasino[5,6] · Julio Saavedra[7] · Edgardo G. Baldo[1] · Juan A. Murra[1] ·
Mario da Costa Campos Neto[4]

Abstract New geochronological, geochemical, and isotopic data are reported for the Capilla del Monte two-mica granite pluton in the northeastern Sierras de Córdoba. An Early Carboniferous age is established by a U–Pb zircon concordia (336 ± 3 Ma) and a Rb–Sr whole-rock isochron (337 ± 2 Ma). Zircon saturation geothermometry indicates relatively high temperatures (735–800 °C). The granites have high average SiO_2 (74.2 %), $Na_2O + K_2O$ (7.8 %), and high field-strength elements, high K_2O/Na_2O (1.7) and FeO/MgO ratios (5.1), with low CaO content (0.71 %). REE patterns with marked negative Eu anomalies (Eu/Eu* 0.14–0.56) indicate crystal fractionation, dominantly of plagioclase and K-feldspar, from a peraluminous magma enriched in F. Isotope data ($^{87}Sr/^{86}Sr_{initial} = 0.7086$, $\varepsilon_{Nd336} = -5.5$ to -4.4 with $T_{DM} = 1.5$ Ga, zircon ε_{Hf336} +0.8 to -6.1; mean $T_{DM} = 1.5$ Ga) suggest a Mesoproterozoic continental source, albeit with some younger or more juvenile material indicated by the Hf data. The pluton is the easternmost member of a Carboniferous A-type magmatic suite which shows an increase in juvenile input toward the west in this part of the pre-Andean margin. The petrological and geochemical data strongly suggest a similar intraplate geodynamic setting to that of the nearby but much larger, Late Devonian, Achala batholith, although Hf isotope signatures of zircon suggest a more uniformly crustal origin for the latter. Further studies are required to understand whether these bodies represent two independent magmatic episodes or more continuous activity.

✉ Juan A. Dahlquist
jdahlquist@efn.uncor.edu

[1] CICTERRA-CONICET-UNC, Av. Vélez Sarsfield 1611, Pab. Geol., X5016CGA Córdoba, Argentina

[2] Visiting Research Associate, British Geological Survey, Keyworth, Nottingham NG12 5GG, UK

[3] CIG-CONICET-UNLP, Calle 1 No. 644, 1900 La Plata, Argentina

[4] Instituto de Geociências da Universidade de São Paulo, Rua do Lago, 562, São Paulo, SP 05508-080, Brazil

[5] INGeReN-CENIIT-UNLaR, Av. Gob. Vernet y Apostol Felipe, 5300 La Rioja, Argentina

[6] CRILAR-CONICET, Entre Ríos y Mendoza, 5301 Anillaco, La Rioja, Argentina

[7] Instituto de Recursos Naturales y Agrobiología de Salamanca (IRNASA, CSIC), Cordel de Merinas, 40-52, Apartado 257, 37008 Salamanca, Spain

Introduction

Geochemical and geochronological studies in the Sierras Pampeanas during the past 15 years have improved our understanding of the petrogenesis and timing of the Pampean and Famatinian granitoids, but Late Paleozoic (i.e., Devonian and Carboniferous) granites emplaced after the metamorphic peak of the Famatinian orogeny have only recently received systematic attention (e.g., Rapela et al. 2008a; Dahlquist et al. 2006, 2010, 2013, 2014a; Alasino et al. 2012 and references therein).

The Late Paleozoic geodynamic setting of this area is still not fully constrained. Based on detailed metamorphic and geochronological analysis, Willner et al. (2011) postulated Late Devonian (~390 Ma) collision of a microcontinent (*Chilenia*) and the subsequent emplacement of Early Carboniferous post-collisional granites to the west. The presence of Carboniferous calc-alkaline granitic rocks in

the Cordillera Frontal has been reported by some authors (e.g., Llambías and Sato 1995; Gregori et al. 1996; Dahlquist et al. 2014a, 2015), but Domeier and Torsvik (2014) affirm that unambiguous evidence of an active pre-Andean margin before the Late Carboniferous (~320 Ma) is still lacking. Recent studies in the Eastern Sierras Pampeanas (e.g., Alasino et al. 2012; Dahlquist et al. 2010, 2013) have shown that the Early Carboniferous granites are typical of A-type metaluminous magmatism with participation of both juvenile material and continental crust in the source, the contribution of the former increasing westwards. Thus, comprehensive studies integrating data for the calc-alkaline and A-type magmatism are required for understanding the Carboniferous geodynamic scenario.

In this paper, we present a precisely defined age by both Rb–Sr whole-rock and U–Pb LA-MC-ICP-MS zircon dating, together with complete petrological characterization, and major and trace element geochemical data for the Capilla del Monte granitic pluton. Rb–Sr and Nd and Hf isotopes are used to constrain the source of parental magma. The geochronological, petrological, geochemical, and isotope data for this pluton are important in that (1) this is the first report of robustly dated Carboniferous magmatism in Sierras de Córdoba, and (2) it is the easternmost example of such magmatism (~1000 km from the present Andean trench).

Geological setting

Using geochronological data and association with known major orogenic episodes, four main granitoid groups have been recognized in the Eastern Sierras Pampeanas. Including main references only, these are *Pampean magmatism*, 555–515 Ma (Rapela et al. 1998, 2007; Sims et al. 1998; Schwartz et al. 2008); *Famatinian magmatism*, 484–463 Ma (Pankhurst et al. 1998, 2000; Rapela et al. 2008b; Dahlquist et al. 2008; Dahlquist and Alasino 2012; Ducea et al. 2010; Casquet et al. 2012); *Achalian magmatism*, 393–366 Ma (Dorais et al. 1997; Sims et al. 1998; Stuart-Smith et al. 1999; Siegesmund et al. 2004); Rapela et al. 2008a; Dahlquist et al. 2014b); and *Early Carboniferous magmatism*, 357–322 Ma (Dahlquist et al. 2006, 2010; Grosse et al. 2009; Alasino et al. 2012). The last group is hereinafter referred to as *Early Gondwana magmatism* following Rapela and Llambías (1999).

Early Gondwana magmatism in the Sierras Pampeanas preceded Late Carboniferous exhumation of deep metamorphic levels formed during the three earlier Paleozoic events and deposition of the continental sediments of the Paganzo Group (Late Carboniferous—Early–Late? Permian, Limarino et al. 2006). Mostly undeformed Early Carboniferous metaluminous A-type granites were emplaced at shallow depth and are dominated by facies with K-feldspar

Fig. 1 Simplified geological map of the Sierras de Cordoba (modified from Baldo et al. 2014) including the Capilla del Monte pluton. *Insets* Location of the Sierras Pampeanas in South America and schematic geological map of Sierras Pampeanas of NW Argentina showing the Paleozoic magmatic development of the pre-Andean margin of SW Gondwana and the setting of the Capilla del Monte pluton (modified from Dahlquist et al. 2013). The *red arrows* indicating the participation of juvenile or continental material are applicable to the Carboniferous magmatism (modified from Alasino et al. 2012). *Pr* Precordillera, *ESP* Eastern Sierras Pampeanas, *WSP* Western Sierras Pampeanas, *Ach* Achala batholith

megacrysts (Dahlquist et al. 2010). They form relatively small, isolated, subcircular plutons scattered throughout the Eastern Sierras Pampeanas without any obvious spatial arrangement (Fig. 1). In many cases, they truncate reactivated shear zones but they never are cut by them (e.g., Dahlquist et al. 2006, 2010).

In the studied region (central NW Argentina, Fig. 1), Early Carboniferous metaluminous A-type granites ranging in age from 322 to 357 Ma (Dahlquist et al. 2013) were emplaced within the continent (now the Eastern Sierras Pampeanas), away from an active plate margin (Alasino et al. 2012). Simultaneously, known calc-alkaline granites were emplaced to the west, in the present-day Western Sierras Pampeanas and Cordillera Frontal (Dahlquist et al. 2015 and references therein). Thus, a geological setting similar to that postulated by Alasino et al. (2012, Fig. 12) including synchronous calc-alkaline and retro-arc A-type magmatism is assumed in this work.

The precise LA-MC-ICP-MS U–Pb zircon crystallization age of 336 ± 3 here reported indicates that the Capilla del Monte pluton was emplaced during Early Carboniferous time, along with the extensive metaluminous A-type magmatism referred to above. In particular, the Capilla del Monte pluton is the easternmost member of the Early Carboniferous A-type magmatic event.

Analytical methods

Samples were collected from the Capilla del Monte pluton for petrographic investigation, whole-rock chemistry, and Rb–Sr analysis during our previous sampling of the Pampean and Famatinian rocks (Rapela et al. 1998). The rocks are assigned to three granitic facies on petrological grounds, as described below. Major element compositions were determined for 12 samples by XRF on fusion pellets and instrumental neutron activation analysis at Activation Laboratories (ACTLABS), Ontario, Canada. A new sample (CAP-1) was collected for U–Pb dating, and this was analyzed for whole-rock major and trace elements using a ThermoARL sequential X-ray fluorescence spectrometer, following the procedure described by Johnson et al. (1999). Trace element compositions were determined using
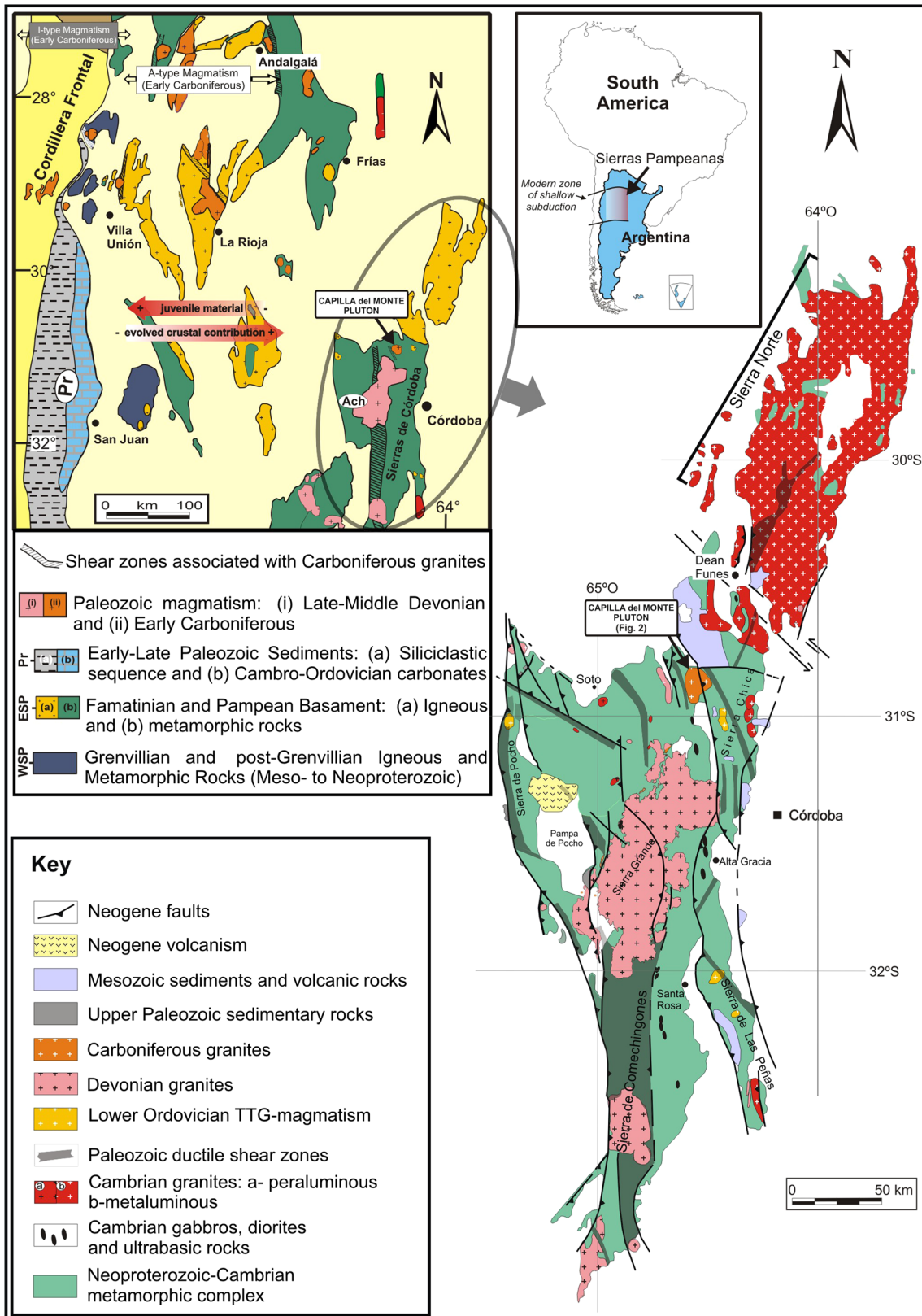
Table 1 Representative major and trace element whole-rock data for the Capilla del Monte pluton

Granitic facies	MME	Facies 1			Facies 2			Facies 3		Aplites			Pegmatite
Samples	CDM 106	CDM 103	CDM 104	CAP 1	CDM 100	CDM 101	CDM 102	CDM 93	CDM 94	CDM 97	CDM 98	CDM 109	CDM 107
wt%													
SiO_2	65.08	73.47	68.37	73.56	75.77	74.65	76.45	75.24	76.21	74.56	75.92	70.90	75.29
TiO_2	1.16	0.30	0.48	0.27	0.12	0.13	0.10	0.11	0.11	0.04	0.03	0.05	0.08
Al_2O_3	14.80	13.40	15.28	13.70	13.51	13.92	13.21	13.76	13.49	14.23	13.93	14.02	13.35
FeO^t	4.82	1.51	2.25	1.33	0.67	0.82	0.68	0.84	0.64	0.43	0.31	0.48	0.26
MnO	0.12	0.07	0.05	0.06	0.09	0.09	0.06	0.08	0.08	0.13	0.06	0.05	0.01
MgO	1.45	0.45	0.69	0.31	0.26	0.07	0.22	0.13	0.10	0.11	0.09	0.00	0.00
CaO	2.56	1.01	1.59	0.82	0.44	0.50	0.47	0.43	0.41	0.50	0.42	0.28	0.21
CaO_{corr}	0.86	0.61	0.92	0.36	−0.23	−0.13	−0.13	−0.30	−0.19				
Na_2O	3.25	2.82	2.89	2.91	2.72	3.06	2.81	2.89	2.75	3.61	3.68	3.16	1.86
K_2O	4.51	4.97	6.14	5.92	4.87	4.57	4.30	4.20	4.36	3.73	3.82	4.56	8.15
P_2O_5	0.51	0.12	0.20	0.14	0.20	0.19	0.18	0.22	0.18	0.23	0.21	0.17	0.00
LOI (%)	0.70	0.35	0.57	0.76	0.79	0.95	0.88	0.66	0.87	0.47	0.75	0.70	0.27
Total	98.96	98.47	98.51	99.78	99.44	98.95	99.36	98.56	99.20	98.04	99.22	94.37	99.48
ppm													
Cs	5	8.4	3.3	7.5	12	13.3	12	8	10	4.7	4.9	4.3	6.2
Rb	363	444	313	426	644	644	600	646	661	658	644	502	550
Sr	250	131	342	151	22	24	21	18	17	18	9	19	115
Ba	510	416	748	507	100	67	120	110	110	110	110	100	230
La	130	55.7	134	68.6	12.2	14	13.3	12.6	13.2	1.9	1.9	2.3	24.4
Ce	265	114	265	142	31	34	33	32	31	5	5	6	52
Pr	nd	nd	nd	16.3	nd	nd	nd	nd	nd	nd	nd	nd	nd
Nd	122	50	106	57	14	14	12	11	10.4	5	5	5	20
Sm	21.2	7.57	14.9	10.44	2.80	2.94	2.80	2.70	2.50	0.60	0.60	0.60	3.30
Eu	2.50	1.11	2.30	1.38	0.20	0.33	0.13	0.30	0.30	0.10	0.10	0.10	1.00
Gd	nd	nd	nd	6.72	nd	nd	nd	nd	nd	nd	nd	nd	nd
Tb	1.90	0.80	1.40	1.01	0.60	0.50	0.50	0.50	0.60	0.50	0.50	0.50	0.50
Dy	nd	nd	nd	5.88	nd	nd	nd	nd	nd	nd	nd	nd	nd
Ho	nd	nd	nd	1.14	nd	nd	nd	nd	nd	nd	nd	nd	nd
Er	nd	nd	nd	3.31	nd	nd	nd	nd	nd	nd	nd	nd	nd
Tm	nd	nd	nd	0.54	nd	nd	nd	nd	nd	nd	nd	nd	nd
Yb	5.00	3.66	3.83	3.63	2.80	2.92	2.80	3.00	3.30	1.60	1.50	1.20	3.60
Lu	0.75	0.55	0.55	0.55	0.42	0.46	0.44	0.46	0.52	0.28	0.26	0.16	0.55
U	9.40	6.70	6.30	7.26	6.40	12.0	7.7	10.0	16.0	6.10	7.50	1.90	21.0

Table 1 continued

Granitic facies	MME	Facies 1		CAP 1	Facies 2			Facies 3		Aplites			Pegmatite
Samples	CDM 106	CDM 103	CDM 104	CAP 1	CDM 100	CDM 101	CDM 102	CDM 93	CDM 94	CDM 97	CDM 98	CDM 109	CDM 107
Th	54.0	36.8	69.8	50.7	13.0	14.3	14.0	13.0	14.0	5.60	5.20	2.30	16.0
Y	74.0	42.0	46.0	31.9	36.0	38.0	39.0	42.0	35.0	26.0	25.0	19.0	29.0
Nb	42.0	43.0	29.0	31.8	64.0	64.0	52.0	67.0	54.0	30.0	29.0	38.0	24.0
Zr	379	163	263	158	66	67	64	65	60	30	28	28	29
Hf	9.00	4.00	8.10	4.82	2.00	2.00	2.20	1.90	1.90	0.90	0.60	1.20	0.70
Pb	57	50	61	61.5	24	24	22	29	31	21	18	20	83
Ta	2	4.2	2.4	3.23	5	6.2	4	5	4	2	2	7	3
Ga	27	23	26	21	36	36	31	35	36	42	38	36	21
X_{Fe}	0.77	0.77	0.77	0.81	0.72	0.92	0.76	0.87	0.86				
$K_2O + Na_2O$	7.76	7.79	9.03	8.83	7.59	7.63	7.11	7.09	7.11				
K_2O/Na_2O	1.39	1.76	2.12	2.03	1.79	1.49	1.53	1.45	1.59				
Al ppm	78,326	70,916	80,866	72,504	71,499	73,668	69,911	72,822	71,393				
$(La/Yb)_N$	17.39	10.18	23.40	12.63	2.91	3.21	3.18	2.81	2.67				
Eu/Eu^*	0.44	0.51	0.56	0.51	0.20	0.33	0.14	0.32	0.32				
$10^4 \times Ga/Al$	3.45	3.24	3.22	2.90	5.04	4.89	4.43	4.81	5.04				
ASI	1.00	1.13	1.07	1.08	1.28	1.28	1.30	1.37	1.37				
ASI_{corr}	1.26	1.20	1.17	1.16	1.45	1.43	1.46	1.57	1.54				
AI	0.69	0.75	0.75	0.82	0.72	0.72	0.70	0.68	0.69				
M	1.81	1.27	1.46	1.33	1.09	1.10	1.06	1.02	1.02				
T_{Zr}		797	836	790	735	735	735	738	732				

Major element oxides and trace elements were analyzed by ACTLABS, Canada, with exception of CAP-1 analyzed in GeoAnalytical Laboratory, WSU, USA (analytical details are found in analytical methods section). Total iron as FeO; major element oxides in wt%, trace elements in ppm. $X_{Fe} = FeO/(FeO' + MgO)$. Different ratios as well as ASI, AI, and T_{Zr} values are calculated for monzogranites facies and granodiorite MME only one. Facies 1: porphyritic monzogranites, Facies 2: equigranular monzogranites with sporadic phenocrystals, Facies 3: Equigranular facies

T_{Zr} (°C) was calculated following Miller et al. (2003) and Dahlquist et al. (2010). Geothermometer was calibrated for $M = 0.9$–1.7. All granitic rocks are monzogranites according to the G1 – G2 – G3 + G4 multicationic classification (homologous to the modal classification of Streckeisen 1976) of de La Roche (1992). ASI Aluminum Saturation Indices = $Al_2O_3/(CaO + Na_2O + K_2O)$ (mol). ASI_{corr} = All ASI values calculated using CaO_{corr}. CaO_{corr} = All CaO values assume all P_2O_5 is in apatite, $CaO_{corr} = CaO - 3.33 \times P_2O_5$

Gd value included in the Fig. 6 was estimated by interpolation using the following calculation model, $Gd_N = (Sm_N \cdot Tb_N^2)^{1/3}$, with exception of CAP-1

MME mafic microgranular enclaves, *nd* not determined

Table 2 Rb–Sr and Sm–Nd data for Capilla del Monte pluton

Sample	Rock type	Rb ppm	Sr ppm	^{87}Rb/^{86}Sr	1σ (%)	^{87}Sr/^{86}Sr	1σ (%)
CDM-93	EG, Facies 3	646	17.7	111.0	1.3	1.2340	0.03
CDM-94	EG, Facies 3	661	16.6	122.3	1.4	1.2960	0.03
CDM-97	Aplite	658	17.6	113.6	1.3	1.2530	0.03
CDM-98	Aplite	644	9.2	223.0	2.0	1.7700	0.04
CDM-100	EG, Facies 2	644	21.9	88.5	1.2	1.1340	0.025
CDM-101	EG, Facies 2	644	23.5	82.2	1.1	1.1020	0.025
CDM-102	EG, Facies 2	599	20.5	88.0	1.2	1.1310	0.025
CDM-103	PG, Facies 1	444	131	9.86	0.5	0.7562	0.01
CDM-104	PG, Facies 1	313	342	2.65	0.5	0.7212	0.01
CDM-106	MME	363	250	4.21	0.5	0.7289	0.01
CDM-107	Pegmatite	550	115	13.94	0.5	0.7748	0.01
CDM-109	Aplite	502	18.8	80.2	1.3	1.0940	0.025

Sample	Rock type	Sm ppm	Nd ppm	^{147}Sm/^{144}Nd	^{143}Nd/^{144}Nd	εNdt	T_{DM}* (Ma)
CDM-94	EG, Facies 3	2.5	10.4	0.1453	0.512244	−5.5	1530
CDM-106	MME	21.2	122.4	0.1047	0.512210	−4.4	1450

PG porphyritic granite, *EG* equigranular granite, *MME* mafic microgranular enclave

$t = 336$ Ma, T_{DM}* after DePaolo et al. (1991)

ICP-MS, following the procedure described in http://www.sees.wsu.edu/Geolab/note/icpms.html. All whole-rock chemistry analyses are included in Table 1.

LA-ICP-MS analysis of separated zircons from sample CAP-1 was carried out at the Geochronological Research Center, Sao Paulo University, Brazil, using a 193-nm excimer laser (Photon Machines) coupled to a Neptune multicollector, double-focusing, magnetic sector ICP-MS. Operating procedures and parameters are discussed by Sato et al. (2011). Fractionation in the plasma was corrected by normalizing U/Pb and Pb/Pb ratios of the unknowns to those of zircon standards (GJ 1, ^{206}Pb/^{238}Pb age by IDTIMS = 599.8 ± 2.4 Ma).

Rb and Sr analyses were carried out at the NERC Isotope Geosciences Laboratory, Keyworth, UK, during the same period as results reported by Rapela et al. (1998). Rb, Sr, and Rb/Sr ratios were determined by X-ray fluorescence on pressed powder pellets calibrated against USGS international standards (Pankhurst and O'Nions 1973), a method that provided consistent accuracy over decades of systematic use. The precision of Rb/Sr ratios, generally ±0.5 %, is primarily dependent on counting-rate statistics and was estimated graphically for the low-Sr samples analyzed here. Sr isotope compositions were determined on a Finnegan-MAT 262 mass spectrometer with static multichannel collection; the NBS987 standard at the time gave a mean ^{87}Sr/^{86}Sr ratio of 0.71020 ± 0.00002. The overall reproducibility of ^{87}Sr/^{86}Sr was normally considered to be 0.01 % but increased significantly for values over 0.8 due to sample inhomogeneity and analytical blank: Uncertainties in Table 2 are empirical estimates. Errors on calculated ages are quoted as 2σ.

Two samples were analyzed for Sm–Nd systematics (using the same mass spectrometric methods as in Rapela et al. 1998). Sm/Nd ratios are precise to ±0.1 % and ^{143}Nd/^{144}Nd to ±0.005 % (1σ).

In situ LA-MC-ICP-MS Lu–Hf isotope analyses were conducted at Geochronological Research Center, Sao Paulo University, Brazil, using a Photon laser system (Sato et al. 2010) coupled to a Thermo-Finnigan Neptune MC-ICP-MS with nine Faraday collectors. Lu–Hf isotopic analyses reported here were performed on the same zircon domains that were previously dated. The laser spot used was 47 μm in diameter with an ablation time of 60 s and a repetition rate of 7 Hz, and He was the carrier gas (Sato et al. 2009, 2010). ^{176}Hf/^{177}Hf ratios were normalized to ^{179}Hf/^{177}Hf = 0.7325. The isotopes ^{172}Yb, ^{173}Yb, ^{175}Lu, ^{177}Hf, ^{178}Hf, ^{179}Hf, ^{180}Hf, and ^{176}(Hf + Yb + Lu) were collected simultaneously. A ^{176}Lu/^{175}Lu ratio of 0.02669 was used to calculate ^{176}Lu/^{177}Hf. Mass bias corrections of Lu–Hf isotopic ratios were according to variation in the GJ1 standard (Basei et al. 2013). Laser operating conditions and results are reported in Table 4.

Petrological characteristics of the Capilla del Monte pluton

Host rocks

The Capilla del Monte pluton is located in the northern part of the Punilla valley (Figs. 1, 2). It was emplaced discordantly in the Early Cambrian La Falda metamorphic
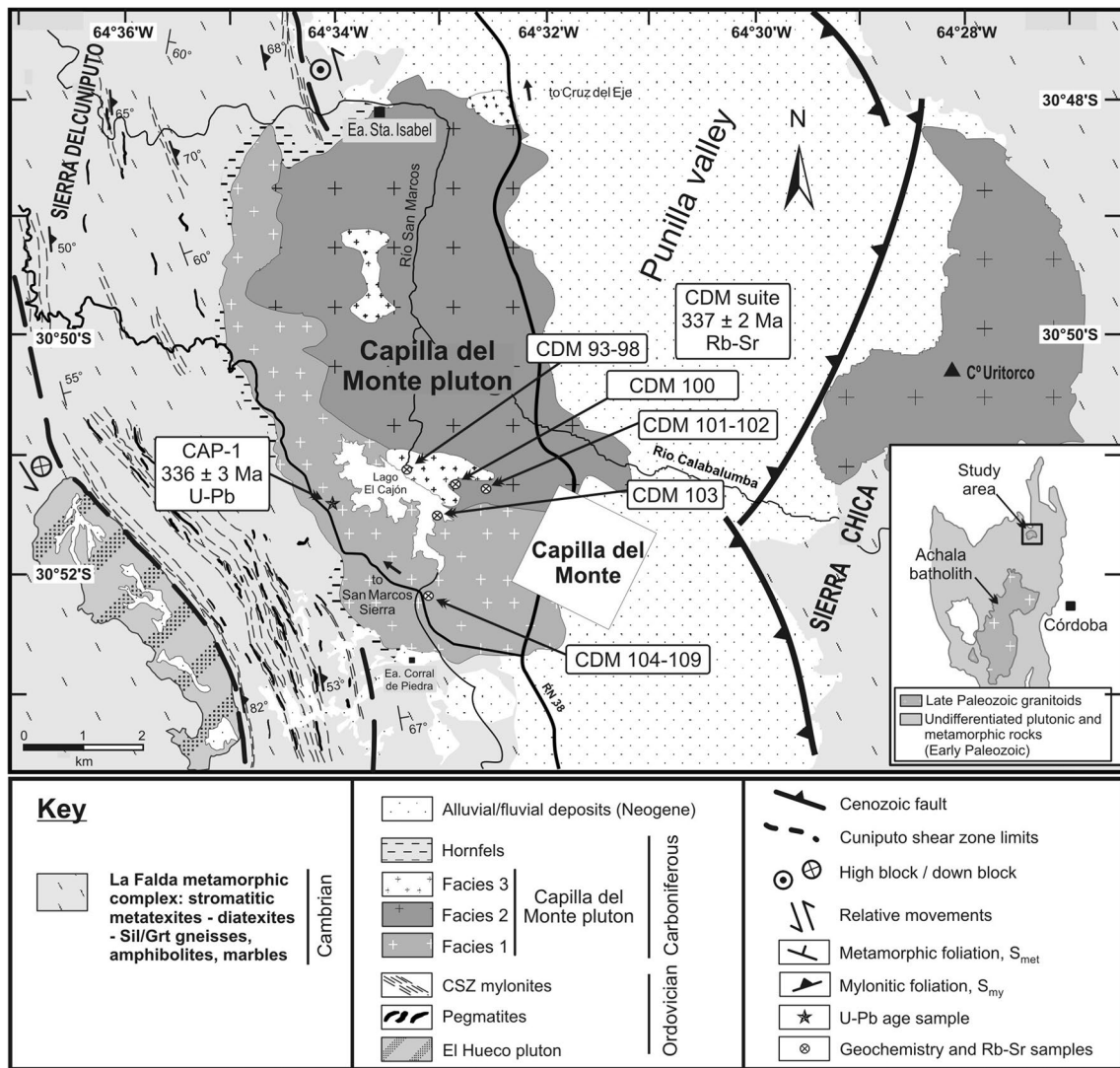
Fig. 2 Geological map of Capilla del Monte pluton (modified from Murra and Baldo 1996). *CSZ* Cuniputo shear zone

complex, which displays a mean metamorphic foliation $S_2 = 350°/60°$ E (Murra and Baldo 1996; Lyons et al. 1997; Candiani et al. 2001). The metamorphic complex includes tonalitic orthogneiss, biotitic gneiss (Kfs–Grt/Sil, mineral abbreviations from Whitney and Evans 2010), stromatitic metatexite and diatexite (Sil − Kfs − Grt ± Crd), ortho-amphibolite (Hbl − Di/Cum), and scattered marble bodies. The metamorphic units are affected by the Cuniputo shear zone (mean S_{myl}: 355°/55° E), which has inverse kinematics and a slight sinistral component (Bellone and Murra 2014). The Cuniputo shear zone is partly cut by the granite, and in various sectors close to the contact, a recrystallized granoblastic gneiss (Qtz − Pl − Kfs − Bt, but no garnet) was recognized.

The Cenozoic Punilla fault led to the rise of the Sierra Chica mountain ranges, resulting in strong topographic relief: The eastern region was raised, forming Cerro

Uritorco, 1949 m above sea level, Fig. 2), while the western sector forms the northwestern region of the Punilla valley. The Capilla del Monte pluton is in the valley section, and its central part is covered by Cenozoic sediments.

The igneous rocks

Three facies of the granitic rocks were recognized by Murra and Baldo (1996) (Fig. 2). Facies 1, located in the southwestern area of the pluton (Fig. 2), is porphyritic monzogranite, with 5- to 7-cm K-feldspar megacrysts in an equigranular matrix formed of quartz (21 %), plagioclase (28 %), poikilitic microcline (40 %), biotite plus musco-vite (11 %), with zircon, monazite, apatite, and opaque as accessories. K-feldspar defines a magmatic foliation par-allel to the contact with the metamorphic host rock. Mafic microgranular enclaves are recognized only in this facies.

They have subspherical form (15 × 7 cm, 60 × 30 cm), with granodioritic composition, strongly enriched in biotite (46–56 %), with apatite, zircon, fluorite, and rutile as accessories. K-feldspar megacrysts similar to those observed in Facies 1 occur in the granodiorite enclaves.

Facies 2 is located in the northeastern and eastern areas (Fig. 2) and is the most abundant. It is a medium-grained equigranular monzogranite with sporadic K-feldspar megacrysts ranging from 1 to 2 cm. The magmatic assemblage is formed by microcline (28 %), quartz (32 %), plagioclase (26 %), muscovite (13 %), and minor biotite. Zircon, apatite, fluorite, and opaque are accessories.

Facies 3 occurs as small-scale bodies located in different parts of the pluton, albeit mostly within the Facies 2 outcrops (Fig. 2). It is a leucocratic monzogranite with quartz (43 %), plagioclase (24 %), microcline (25 %), and muscovite (9 %), with zircon, apatite, and opaque as accessories mineral, but biotite is absent. The outcrop disposition and the analytical results reported here are consistent with Facies 3 being a minor variant of Facies 2.

Feldspathic aplite dykes and tabular granitic pegmatites cut the granitic rocks. The pegmatites contain muscovite, biotite, beryl, triplite, and apatite. Small, centimetric, fluorite dykes in Facies 2 have been reported by Agulleiro Insúa et al. (2013).

Whole-rock chemical composition

Major elements

The data show that all the granitic rocks are monzogranite, and their SiO_2 content varies within a restricted range from 68 to 76 % (Table 1). A representative analysis from one sample of a mafic microgranular enclave (MME) in Facies 1 is also reported in Table 1.

In the alkalis versus silica classification diagram of Wilson (1989), the data plot mainly within the Carboniferous A-type granite field of the Sierras Pampeanas, and some samples are close to other typical A-type granites reported in the literature. The Capilla del Monte pluton includes subalkaline monzogranite enriched in alkalis (Facies 2 and 3) and mid-alkaline monzogranite (Facies 1) (Fig. 3a). The plot differentiates the Capilla del Monte granites from those of the Ordovician calc-alkaline monzogranites; their high K_2O contents are similar to those of other Carboniferous A-type granites in the Sierras Pampeanas (Dahlquist et al. 2010). The enclave has granodioritic composition but also with distinctive alkali enrichment.

The monzogranite samples are poor in calcium (CaO < 1.6 % in Facies 1 and <0.5 % in Facies 2 and 3) and their high total alkalis (7.10–9.03 %) with K_2O/Na_2O ratios of 1.50–2.12 mean that they also plot mainly in
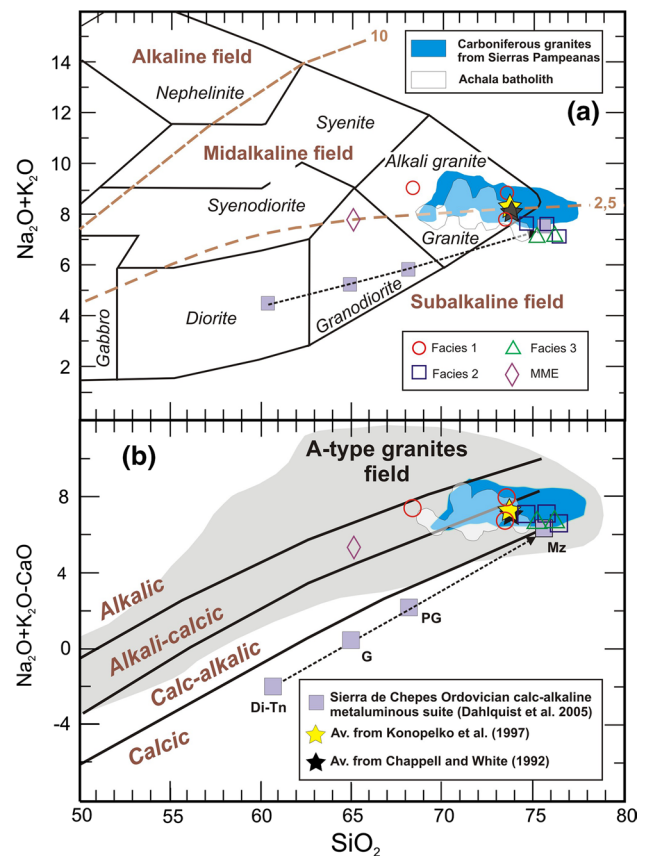

Fig. 3 **a** Alkali–silica diagram for the Capilla del Monte pluton samples (MME = microgranodiorite enclave). The fields are 46 Carboniferous granitic samples from the Eastern Sierras Pampeanas (Dahlquist et al. 2010) and 18 granitic samples of the Achala batholith (Dahlquist et al. 2014b). The *star* symbols are averages for A-type granites in other parts of the world, as indicated. The alkaline/midalkaline/subalkaline magmatic lineages are defined by sigma isopleths (after Rittmann 1957). **b** $Na_2O + K_2O - CaO$ versus SiO_2. The A-type granitoid field is after Frost et al. (2001). Representative data for the Sierra de Chepes (Famatinian) calc-alkaline suite are plotted in both diagrams for comparison: *Di–Tn* diorites and tonalites, *G* granodiorites, *PG* porphyritic granodiorites, *Mz* monzogranites

the same field as other Sierras Pampeanas Carboniferous A-type granites. They range from alkali-calcic to calc-alkaline in the $Na_2O + K_2O - CaO$ versus SiO_2 diagram of Frost et al. (2001) (Fig. 3b). The granodiorite MME data plot in the alkali-calcic field. All samples are extremely rich in FeO^t, with high $FeO^t/(FeO^t + MgO)$ ratios (0.72–0.92, average = 0.80), comparable to those commonly observed in A-type granite (i.e., >0.7, e.g., Anderson 1983; Whalen et al. 1987; Dahlquist et al. 2010).

Finally, all facies are peraluminous, with alumina saturation index (ASI) ranging from 1.16–1.57 (Fig. 4 and Table 1) and with a relatively high agpaitic index of 0.68–0.82, of which the lowest values are in Facies 3 (Table 1). The granodiorite enclave is also peraluminous (ASI = 1.26).
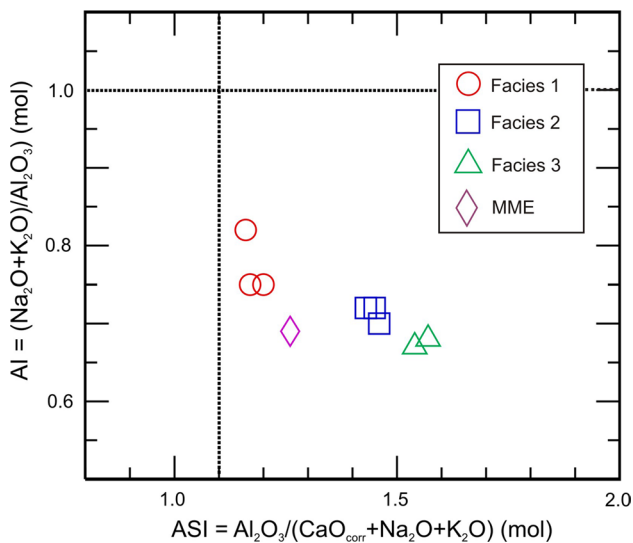
Fig. 4 Alumina saturation index (ASI) in the studied granitic rocks. An ASI_{corr} value is used in the figure (calculation model is shown in Table 1). All granitic facies are peraluminous and have relatively high values for the agpaitic index (AI). The ASI limit is taken as either 1.0 (Shand 1927) or, as shown, 1.1 (Chappell and White 1992).
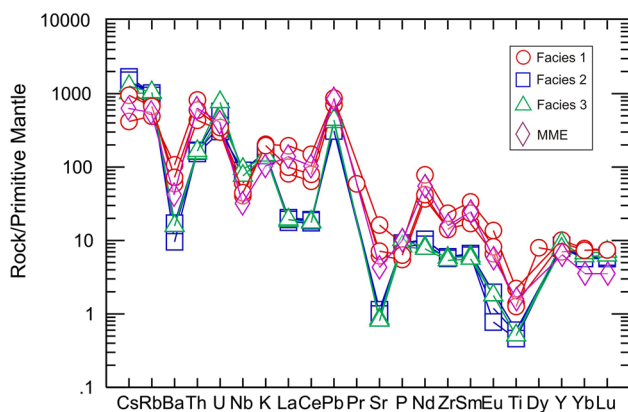

Fig. 6 Chondrite-normalized (Nakamura 1974; Boynton 1984) REE plots. **a** The rocks of the Capilla del Monte pluton have REE patterns similar to those reported for Carboniferous A-type granites by Dahlquist et al. (2010). **b** REE patterns for the Los Árboles pluton, a comparable Carboniferous A-type granite in the Sierras Pampeanas. Note that the Eu anomaly becomes more negative, and the SiO_2 content increases from the porphyritic (*western zone*) to the equigranular (*eastern zone*) facies, as observed in the Capilla del Monte pluton

Fig. 5 Primitive mantle-normalized (Sun and McDonough 1989) spider diagrams. The granitic rocks of the Capilla del Monte pluton have similar compositions to those reported for Carboniferous A-type granites of the Sierras Pampeanas (see Dahlquist et al. 2010)

Trace elements and REE

All granitic facies have concentrations of high field-strength elements (Y, Nb, Ga, Ta, U, Th, LREE, etc.) comparable to those reported for metaluminous A-type granitic complexes, such as the A-type granites of the Lachlan Fold Belt in Australia, the Hercynian Kokshaal range in Kyrgyzstan, and elsewhere in the Sierras Pampeanas of Argentina (see data in Table 1 of Dahlquist et al. 2010). Primitive mantle-normalized spider diagrams for Facies 1 show
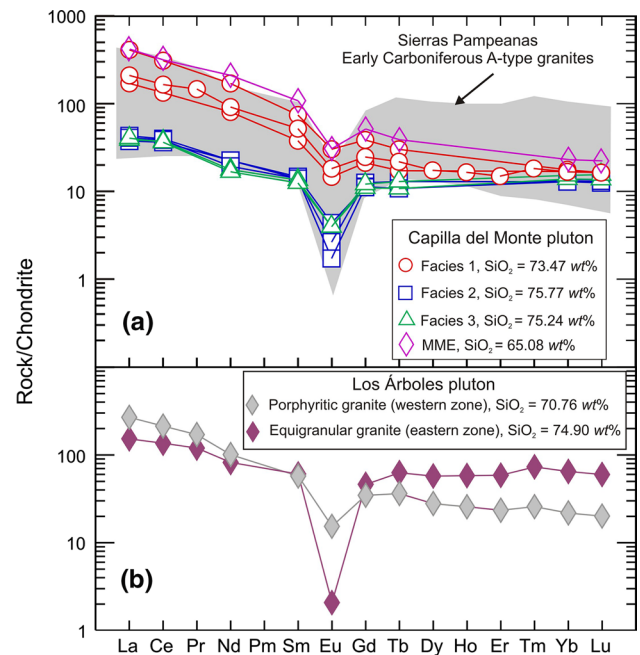
marked negative Ba, Nb, Sr, P, Eu, and Ti anomalies and unusual enrichment in Cs, Rb, Th, U, and Pb for metaluminous granitoids (Fig. 5). Facies 2 and 3 have patterns that are indistinguishable from each other, with markedly lower Ba, La, Ce, Sr, and Zr contents than Facies 1. In Facies 1, the light rare earth elements (LREE) are strongly enriched, with negative Eu anomalies (mean Eu/Eu* = 0.53) and La_N/Yb_N ratios of ca. 10–24 (Fig. 6a). The REE patterns of Facies 2 and 3 are again closely similar to each other, but distinct from those of Facies 1, with lower LREE concentrations and much lower La_N/Yb_N ratios of 2.7–3.2, as well as even stronger Eu anomalies (mean Eu/Eu* = 0.27), suggesting a greater degree of feldspar fractionation. In general, the range of REE patterns shown by all three facies is similar to that of other Early Carboniferous A-type granites of the Sierras Pampeanas (Dahlquist et al. 2010). In particular, there is a close resemblance to those of the Los Árboles pluton (Fig. 6b), one such granite with two distinctive facies: porphyritic (western zone) and equigranular (eastern zone), suggesting a similar differentiation process. As in the case of major elements, the granodiorite MME has a similar composition to the granitic rocks of Facies 1 (Figs. 5, 6a).

Geochronological data and isotope signature of the Capilla del Monte pluton

Previous geochronological data

The first Late Paleozoic ages for the granitic rocks of Sierra de Córdoba (380–373 Ma) were obtained by Linares (1966), using Pbα methodology. Subsequently, Linares and Latorre (1969) and Massabie (1982) reported Devonian and Carboniferous K–Ar ages on whole rocks (380–336 Ma), biotite (346 Ma), and muscovite (376–334 Ma). A rough Early Carboniferous age (337 ± 30 Ma, Rb–Sr whole rock) was obtained by Rapela et al. (1991) from the Characato porphyritic granite, in the northwestern part of the Achala batholith.

Rb–Sr whole-rock age and Nd isotopes

The samples from the Capilla del Monte pluton are enriched in Rb, with whole-rock contents of mostly 500–700 ppm (Table 2). Two porphyritic granite samples (Facies 1), the microgranodioritic enclave and the pegmatite, all have high Sr contents (115–342 ppm), but the remaining granites (Facies 2 and 3) and aplites contain less than 25 ppm, resulting in a wide range of Rb/Sr ratios. The seven granite samples alone fall on an isochron corresponding to an age of 338 ± 3 Ma (MSWD = 0.6), but the complete data set also defines an indistinguishable isochron (MSWD = 0.8), with an age of 337 ± 2 Ma and an initial $^{87}Sr/^{86}Sr$ of 0.7086 ± 0.0002 (Fig. 7). This is taken as indicating that all these rocks had a co-magmatic origin, and that the Rb–Sr age records whole-rock system closure immediately after crystallization of the pluton.

The Sm–Nd analyses for a Facies 3 equigranular granite and the granodiorite mafic microgranular enclave (Table 1, 2b) are also reasonably consistent, with ε_{Ndt} values of −5.5 and −4.4, respectively, and corresponding depleted mantle model ages assuming a crustal source (DePaolo et al. 1991) of 1.53 and 1.45 Ga.

U–Pb LA-MC-ICP-MS zircon age and Hf isotope data

The combined SEM-CL and optical images reveal that the zircon grains separated from sample CAP-1 are mostly prismatic elongate with oscillatory zoning and subhedral to euhedral terminations. Analysis spots were mostly located on outer oscillatory zoning, and the majority of the zircon ages are concentrated at about 336 Ma (Table 3). Sixteen data points yield a Tera-Wasserburg concordia age (Ludwig 2003) of 336 ± 3 Ma (95 % confidence limits, allowing for the uncertainty in U/Pb calibration). This is considered the best estimate for the crystallization of the host monzogranite (Fig. 8). The Early Carboniferous zircon grains have
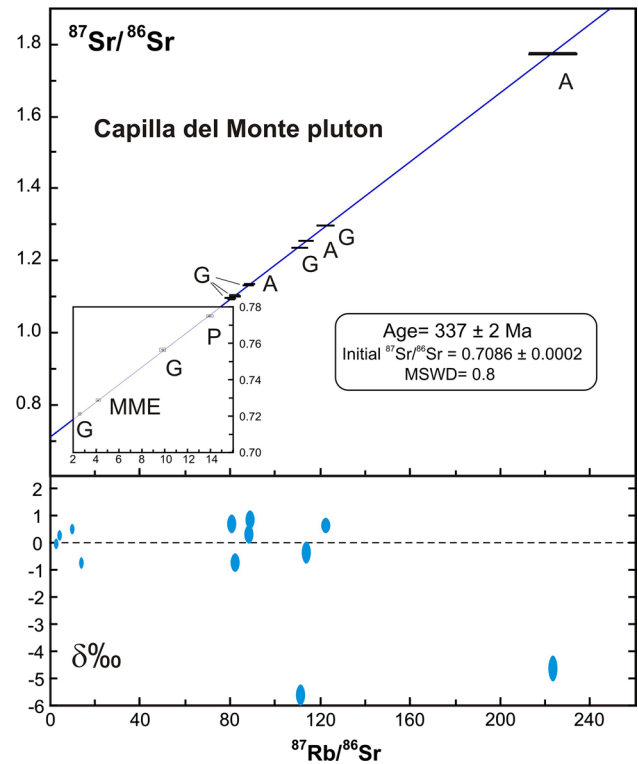

Fig. 7 Rb–Sr isochron plots. Samples are mafic microgranular enclave (*MME*), granite (*G*), pegmatite (*P*), and aplite (*A*). The data and facies assignments are given in Table 2. Note the expanded scale for the *inset box*. Since error ellipses are mostly too small to display, the lower part of the diagram shows permil deviations (δ) from ideal points on the isochron corresponding to the measured Rb/Sr ratios

variable ε_{Hft} ($t = 336$ Ma) values, ranging from +0.8 (the only positive value) to −6.1. The average Hf model age is calculated as 1.46 Ga (Table 4; Fig. 9).

Discussion: genesis of the Carboniferous granites

Magmatic fractionation in the Capilla del Monte pluton

The zircon geothermometer of Watson and Harrison (1983) was used to estimate magmatic temperatures, since Miller et al. (2003) conclude that this is applicable to both inheritance-rich and inheritance-poor granitoids. The average calculated temperatures for *M* values between 0.9 and 1.7 (the calibration range for the geothermometer) are 805 °C for Facies 1 (porphyritic monzogranite) and 735 °C for Facies 2 (equigranular ± porphyritic monzogranite); Facies 3 yields similar temperatures to Facies 2 (Table 1). These temperatures are consistent with those obtained from other Carboniferous A-type granites in the Sierras Pampeanas (Dahlquist et al. 2010). Comparing the results for the different facies, temperature decreases as the Eu anomaly

Table 3 LA-MC-ICP-MS results for CAP-1 monzogranite zircon (Facies 1)

Grain spot	GCh SS	Ratios				Ages			
		$^{238}U/^{206}Pb$	1σ	$^{207}Pb/^{206}Pb$	1σ	$^{206}Pb/^{238}U$	1σ	$^{207}Pb/^{206}Pb$	1σ
11.1	e, p, osc	19.4457	0.2583	0.0539	0.0020	323	4	368	84
22.1	e, p, osc	19.2777	0.4132	0.0544	0.0022	326	7	389	95
7.1	e, p, osc	18.9537	0.4736	0.0495	0.0047	331	8	170	181
23.1	e, p, osc	18.9513	0.3307	0.0528	0.0017	331	6	319	68
13.1	e, p, osc	18.9039	0.2573	0.0536	0.0019	332	4	355	81
10.1	e, p, osc	18.8793	0.2160	0.0538	0.0014	333	4	365	59
16.1	e, p, osc	18.8583	0.9547	0.0475	0.0070	333	16	74	210
3.1	e, p, osc	18.7854	0.2821	0.0523	0.0025	334	5	297	106
20.1	e, p, osc	18.8180	0.3348	0.0534	0.0018	334	6	348	76
2.1	e, p, osc	18.6722	0.3346	0.0504	0.0031	336	6	212	131
17.1	e, p, osc	18.4973	0.3284	0.0539	0.0017	339	6	365	73
9.1	e, p, osc	18.4334	0.3306	0.0508	0.0032	341	6	232	139
18.1	e, p/fr, osc	18.3838	0.9206	0.0524	0.0068	341	17	301	205
14.1	e, p, osc	18.3769	0.4044	0.0517	0.0023	342	7	273	106
12.1	e, p, osc	18.2758	0.4215	0.0500	0.0045	343	8	195	158
6.1	e, p, osc	18.0415	0.2223	0.0538	0.0017	348	4	362	72
24.1	e, p, osc	17.4984	0.4707	0.0517	0.0032	358	9	273	123

^{238}U/^{206}Pb and ^{207}Pb/^{206}Pb ratios corrected for static fractionation using GJ 1

Measurement errors represent within-run uncertainty only. Grain characteristics (GCh) and site of the spot (SS): site of the spot: *e* end or edge. Habit of the grain: *p* prism, *fr* fragmented. CL images: *osc* oscillatory zoning
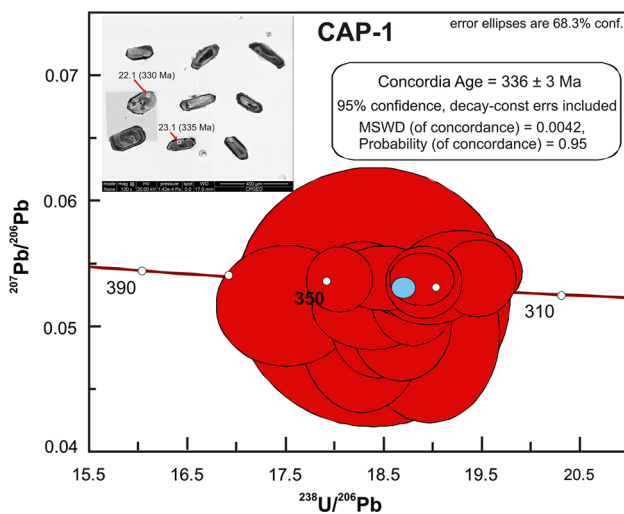

Fig. 8 U–Pb LA-MC-ICP-MS zircon dating of sample CAP-1 (Facies 1 monzogranite) from the Capilla del Monte pluton. The main Tera-Wasserburg plot shows most analyses plotting between 323 and 358 Ma, and the *inset* shows a concordia age calculation of 336 ± 3 Ma. Selected zircon images are also shown. Data are reported in Table 3

becomes more negative, and the SiO$_2$ content increases (Table 1), consistent with increased differentiation.

The fact that Rb–Sr data for all samples, including all three granite facies, aplites, and a granodiorite enclave, lie on a single well-defined isochron is taken as indicating that all these rocks share a co-magmatic origin with closure of the Rb–Sr whole-rock system immediately after crystallization of the pluton. This also strongly suggests that the muscovite was a primary magmatic phase, or that at least that there was no secondary growth involving external fluid exchange. The granodiorite MME has the lowest SiO$_2$ content in the pluton and may represent early segregation from a granitic magma, but more data are required to test this.

The decrease in LREE contents and La$_N$/Yb$_N$ ratios, coupled with more pronounced negative Eu anomalies, as SiO$_2$ increases from Facies 1 to Facies 2 and 3 (Fig. 6a), suggests that the main factor in the differentiation process was feldspar fractionation, together with accessory minerals such as monazite. The parallel development of negative Ba and Sr anomalies in the spider diagrams similarly supports the important role of feldspar (Fig. 10a, b). Since Ba is not significantly partitioned into plagioclase, it is probable that K-feldspar (plus biotite) was an important crystallizing phase in Facies 1, and it is notable that there is also a slight fall in K$_2$O in Facies 2 and 3 (Table 1). On the other hand, the higher CaO content (together with Sr and Eu) in Facies 1 relative to Facies 2 and 3 (almost 3 times, Table 1) suggests that An-rich plagioclase fractionation was also involved. Simple vectors calculated for Ba and Rb are consistent with two possible crystallization stages during differentiation of the Capilla del Monte magma: Kfs ≫ Pl

Table 4 Laser ablation Hf isotope data for igneous dated zircons from CAP-1

Grain/spot	$^{176}Hf/^{177}Hf$	$\pm 2\sigma$	$^{176}Lu/^{177}Hf$	$\pm 2\sigma$	εHf (t)	T_{DM} (Ga)
3.1	0.282594	0.000056	0.001323	0.000042	0.79	1.24
6.1	0.282426	0.000051	0.001143	0.000038	−5.09	1.61
10.1	0.282488	0.000029	0.001069	0.000007	−2.90	1.47
11.1	0.282518	0.000037	0.000854	0.000028	−1.78	1.40
13.1	0.282519	0.000040	0.000819	0.000010	−1.73	1.40
14.1	0.282493	0.000043	0.001075	0.000004	−2.69	1.46
17.1	0.282536	0.000052	0.000722	0.000023	−1.11	1.36
18.1	0.282438	0.000058	0.001469	0.000007	−4.74	1.59
20.1	0.282520	0.000038	0.001356	0.000014	−1.82	1.40
22.1	0.282508	0.000050	0.001090	0.000013	−2.19	1.43
23.1	0.282403	0.000060	0.002150	0.000027	−6.12	1.68

Laser operating conditions: GJ1—6 mJ ou 8.55 J/cm2 (100 %), 7 Hz, spot = 47 um, He (MCF1) = 0.25 l/min (MCF2) = 0.5 L/min, N_2 = 1.2 mL/min, 50 ciclos, AR80 = 30 V

t = crystallization age (336 Ma), T = model age

Present-day and initial ε_{Hft} values were calculated using CHUR compositions of $^{176}Hf/^{177}Hf_{today}$ = 0.282772 and $^{176}Lu/^{177}Hf$ = 0.0332 (Blichert-Toft and Albarede 1997) and a ^{176}Lu decay constant of $1.867e^{-11}$ (Söderlund et al. 2004; Scherer et al. 2007). Average crustal $^{176}Lu/^{177}Hf$ of 0.015 (Goodge and Vervoort 2006). Depleted mantle (DM) parameters from (Vervoort and Blichert-Toft 1999). $^{176}Hf/^{177}Hf_{CHUR(t)}$ = 0.282563

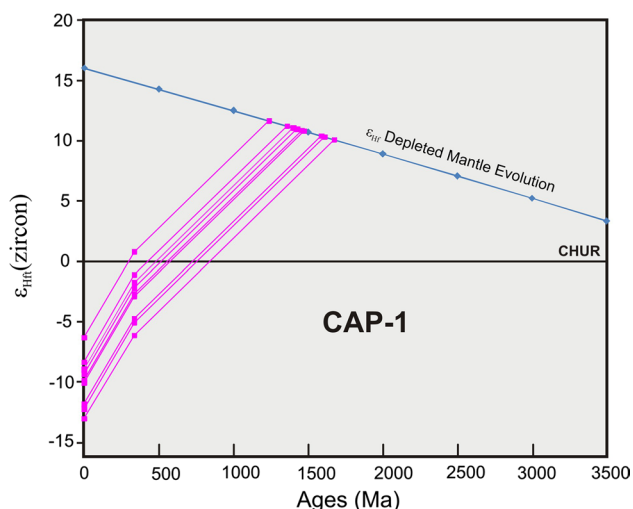**Fig. 9** Age versus ε_{Hft} values for Early Carboniferous zircon hosted in CAP-1 granite, showing both measured and initial epsilon Hf values as function of crystallization age. Depleted mantle Hf evolution curve from Vervoort and Blichert-Toft (1999) and pre-crystallization average crustal growth parameters from Goodge and Vervoort (2006)

during the crystallization of Facies 1, and Pl ≫ Kfs during the subsequent crystallization of Facies 2 and 3 (Fig. 9c). This is consistent with the thermometry calculation and geochemical variations summarized above.

The concomitant decrease in LREE, Ti, Zr, and Th (Fig. 5), further implies segregation of accessory minerals such as Ti oxides, zircon, and monazite, whereas as Rb, Cs, and U were enriched in the more differentiated magma,

probably by selective extraction and transport in a volatile phase (Cerný et al. 1985). This is similar to the crystallization process invoked for other A-type granites of the Sierras Pampeanas (Dahlquist et al. 2010).

High Ga/Al is a distinctive characteristic of A-type granite, and plots against major and trace element contents can readily distinguish between I-type (calc-alkaline) and A-type granite (Whalen et al. 1987). The Ga versus Ga/Al diagram of Fig. 11 shows such a distinction between the Sierras Pampeanas Carboniferous A-type granites and the Ordovician calc-alkaline granites of the Famatinian orogen. Experimental studies by Patiño Douce (1997) indicate that the higher proportion of Ca-rich plagioclase formed by incongruent melting at low-pressure conditions (4 kbar) explains the low CaO relative to Al_2O_3 of metaluminous A-type granites (as well as their Eu depletion), and because plagioclase excludes Ga relative to Al_2O_3 (Malvin and Drake 1987), it also gives rise to their distinctively high Ga/Al ratios. Alternatively, Whalen et al. (1987) indicate that Ga is enriched relative to Al because the latter is preferentially trapped in residual plagioclase, while during melting of an F-enriched source, Ga is stabilized in the melt in GaF_6^{-3} structures. This is consistent with the fact that most Facies 2 granites (and small dykes) include fluorite as an accessory mineral. This is a further characteristic of A-type magmatism (e.g., Collins et al. 1982; Whalen et al. 1987; Dahlquist et al. 2010) and suggests that the Capilla del Monte magmas were derived from a F-rich source. Recently, Agulleiro Insúa et al. (2013) have reported high F contents in the Capilla del Monte pluton, increasing
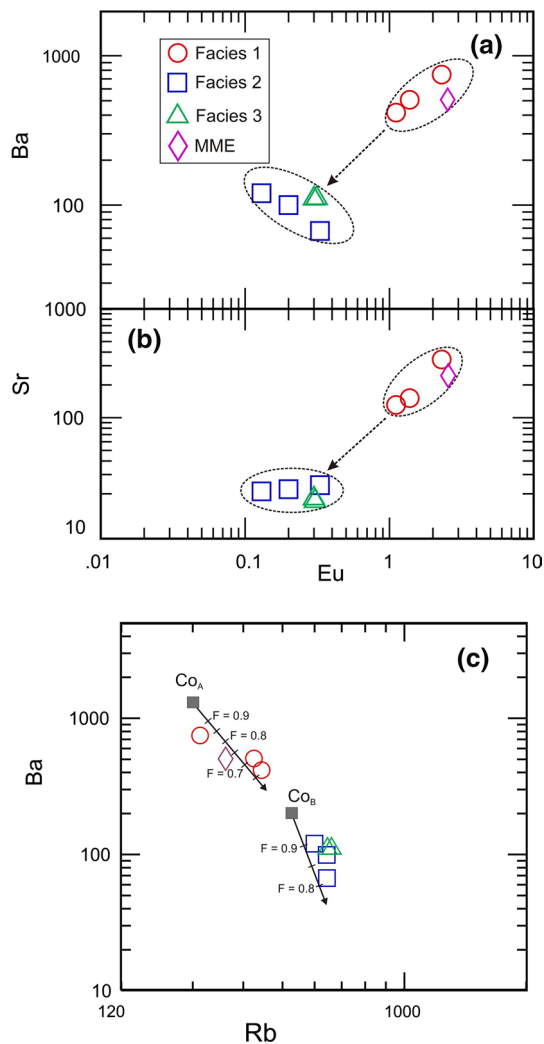
Fig. 10 **a**, **b** Ba versus Eu and Sr versus Eu (concentrations in ppm). Facies 1 has higher contents of these elements, and the trend to lower concentrations in Facies 2 and 3 suggests segregation of plagioclase and K-feldspar. **c** Ba versus Rb. Linear trends for granitic facies of the Capilla del Monte pluton. The calculated vector indicates that K-feldspar (Kfs) and plagioclase (Pl) crystallized in different proportion in Facies 1 (Kfs = 60 % and Pl = 20 %) and Facies 2 and 3 (Kfs = 20 % and Pl = 60 %), respectively. The percentage values are only indicative. Partition coefficient data for minerals in equilibrium with granitic liquids are from Icenhower and London (1996), Ewart and Griffin (1994), Nash and Crecraft (1985), and Streck and Grunder (1997). The crystallization percentage for Kfs and Pl is indicated in the figure. Co_A initial concentration for Facies 1, Co_B initial concentration for Facies 2 and 3, F weight fraction of remaining melt

from 1200 ppm in porphyritic biotite granite (equivalent to our Facies 1) to 2600 ppm in leucogranites with dominant muscovite (equivalent to our Facies 3). García et al. (2012) have reported high F content in water samples from the Calabalumba and San Marcos Rivers that cross the Capilla del Monte outcrop, concluding that it mostly originated through the weathering of F-bearing minerals such as micas, fluorapatite, apatite, and fluorite.
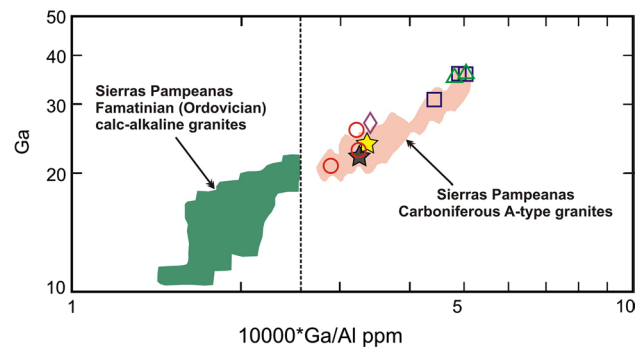

Fig. 11 Ga versus $10^4 \times$ Ga/Al granite discrimination diagram (Whalen et al. 1987) showing granite of the Capilla del Monte pluton compared to the Early Carboniferous A-type granites (Dahlquist et al. 2010) and the Famatinian calc-alkaline granitoids (Dahlquist et al. 2005, 2008). For the Famatinian calc-alkaline granitoids, the SiO_2 content ranges from 60 % (tonalite) to 75 % (monzogranite). The $10^4 \times$ Ga/Al discrimination limit for A-type granites is from Whalen et al. (1987). Stars are A-type average compositions from Konopelko et al. (2007) and Chappell and White (1992), respectively

Source of the granitic magma of Capilla del Monte pluton

The initial $^{87}Sr/^{86}Sr$ ratio of 0.7086 and negative εNdt values ranging from −4.4 to −5.5 indicate that the generation of the Capilla del Monte parental magma dominantly involved crustal melting, with a minimal contribution of juvenile material. The average of two depleted mantle Nd model ages of ca. 1.5 Ga and coincidence with the same model age for most of the zircon Hf analyses strongly suggest a Mesoproterozoic source.

However, ε_{Hft} for magmatic zircon shows a significant spread from crustal values (−6.1) to just positive (+0.8). Thus, whereas the $Sr_{initial}$ and ε_{Ndt} values suggest a single crustal source, the ε_{Hft} values imply interaction between juvenile and continental material, although the latter appears to be dominant. In theory, this could be due to assimilation of younger, more primitive, crustal material or partial involvement of a juvenile magma, although in either case interaction must have occurred prior to differentiation of the magma that produced the exposed pluton in order to account for the uniformity of the Sr and Nd isotope signatures. As in the general study reported by Kemp et al. (2007), an important feature of the Hf isotope data is the significant range of ε_{Hft} values exhibited by zircon within a single sample (up to 10 ε units). Such scatter could be due to some zircon crystallizing very early and retaining vestiges of the original, more juvenile Hf isotope signature (Kemp et al. 2007; Dahlquist et al. 2013), whereas the $^{176}Hf/^{177}Hf$ ratio of the melt from which the early zircon precipitated might change due to subsequent assimilation of crustal material. Alternatively, a heterogeneous crust

could be assumed as the source of the parental magma (Villaros et al. 2012), although again the magma must have become homogenized (apart from the already precipitated zircon) prior to the crystal fractionation process described above.

Recent studies of Early Carboniferous granites in the Eastern Sierras Pampeanas indicate that they represent typical A-type metaluminous magmatism developed in intraplate setting, with participation of both juvenile material and continental crust in the source (Dahlquist et al. 2010). Within the whole suite, the proportion of juvenile material increases toward the west, where the Cerro La Gloria pluton (Fig. 1) has an average zircon ε_{Hft} value of +2.6 (Alasino et al. 2012; Dahlquist et al. 2013). The dominantly continental origin of the Capilla del Monte pluton, which constitutes the easternmost outcrop of the Carboniferous A-type suite (Fig. 1), is consistent with this trend.

Comparison with the Achala batholith and geodynamic implications

Late Devonian and Early Carboniferous geodynamic setting

There are significant doubts about the possible continuity of both granite magmatism and deformation in the Late Devonian to Mid-Carboniferous interval. The ca. 2500-km² Achala batholith in the Sierras de Córdoba (Fig. 1) is a F-rich peraluminous A-type granite (Rapela et al. 2008a, Dahlquist et al. 2014b), and contact aureoles indicate shallow emplacement, usually at less than 2 kb (e.g., Patiño and Patiño Douce 1987; Baldo and Verdecchia 2014). Pinotti et al. (2002) report similar conclusions for the Cerro Áspero batholith, also of Late Devonian age (Fig. 1). The Achala batholith is the largest of a series of intrusive granitic bodies in the Eastern Sierras Pampeanas that are conspicuously discordant to structures and rocks formed during the Cambrian (Pampean) and Ordovician (Famatinian) metamorphic events (Martino et al. 1995; Rapela et al. 2008b). The granites were emplaced during the Late Devonian: 368 ± 25 Ma (U–Pb zircon, Dorais et al. 1997); 379 ± 4 and 369 ± 3 Ma (U–Pb SHRIMP zircon, Rapela et al. 2008a); and 366 ± 6, 369 ± 5, 372 ± 6 Ma, 370 ± 8 (U–Pb LA-MC-ICP-MS zircon, Dahlquist et al. 2013, 2014b). It is possible that different components of this large body crystallized at somewhat different times, but an overall emplacement age of 365–370 Ma would seem well established, whereas the Early Gondwana magmatism spans ca. 357–322 Ma (Dahlquist et al. 2013).

Sims et al. (1998), Stuart-Smith et al. (1999), Siegesmund et al. (2004), and López de Luchi et al. (2004, 2007) considered the voluminous Devonian intrusive rocks in the

Sierras de Córdoba and the eastern area of the Sierra de San Luis to have been emplaced during compression in a transtensional regime associated with Late Devonian low-grade shear zones, together defining the Achalian orogeny (Middle-to-Late Devonian). Sims et al. (1998) used the ^{40}Ar–^{39}Ar step-heating method on biotite that grew during mylonitization, yielding well-defined ages of 358 ± 2 for the Guamanes mylonite (Sierras de Córdoba), and 366 ± 2 and 375 ± 1 for a shear zone in Sierra de San Luis, the latter being essentially coincident with the intrusive age of the Achala granites. Igneous phases of the Achala batholith truncate deformation fabrics of the Tres Árboles fault zone (Fig. 1), which implies that movement along the shear zone must have ceased prior to ca. 365–370 Ma. On the other hand, the Tres Árboles ultramylonites have yielded much younger ^{40}Ar–^{39}Ar ages of 343 ± 5 and 341 ± 5 Ma (Whitmeyer 2008), respectively, although these were interpreted as regional cooling ages and can only be regarded as minimum estimates for the cessation of fault movement. Wemmer et al. (2011) obtained K–Ar ages of 334–291 Ma for fine-grained illite from phyllites associated with shear zones in Sierra de San Luis. They considered that the ages older than 320 Ma correspond to a phase of compressional tectonism linked with the Toco orogeny that is recognized in northern Chile and southern Bolivia. In an extension of that study that included fault gouges from the Sierras Pampeanas, Bense et al. (2014) point out that the Toco orogeny is not clearly displayed in Sierras Pampeanas and concluded that such ages mark a change from ductile to brittle deformation at the end of prolonged Famatinian deformation.

The tectonic setting of the Late Devonian compressional event and the transition to the Carboniferous tectonic setting is thus somewhat controversial, especially regarding the continuity or otherwise of compressional tectonics. Scenarios invoked include (1) collision of the hypothetical Chilenia terrane with the proto-Pacific margin and post-collision extensional magmatism (Willner et al. 2011 and references therein), (2) final collision between the Famatinian magmatic arc and the Pampean hinterland (Höckenreiner et al. 2003), and recently, (3) push–pull tectonic switching along the Pacific margin during Devonian and Carboniferous time (Alasino et al. 2012). The A-type geochemical signature of the Achala batholith (Rapela et al. 2008a; Dahlquist et al. 2014b) strongly suggests intracratonic or within-plate magmatism in a dominantly extensional regime with Early–Middle Devonian lithospheric thinning. This hypothesis is consistent with a Devonian metallogenetic epoch (~390 Ma) developed in a within-plate extensional setting temporally and spatially related to Achala magmatism (Franchini et al. 2005). This intracratonic extensional regime was followed by Late Devonian compression (Sims et al. 1998) and Early Carboniferous

lithospheric stretching (Dahlquist et al. 2010, Alasino et al. 2012). Geochronological dating and subsidence analysis of the Paganzo basin of NW Argentina support an initial rift stage at the time of the Devonian–Carboniferous boundary (Astini et al. 2009, 2011). Thus, tectonic switching episodes of rollback and flat-slab subduction (see Collins 2002) could have led to alternating compression and extension setting in the pre-Andean margin.

It is well known that A-type magmas are formed in a variety of extensional regimes: in continental back-arcs, in post-collisional extension, and in within-plate settings (e.g., Whalen et al. 1987; Eby 1992; Bonin 2007). Experiments by Patiño Douce (1997) show that dehydration of calc-alkaline granitoids in the shallow crust (at depths of 15 km or less) is a likely origin for high-silica metaluminous A-type granites [$(Na_2O + K_2O)/Al_2O_3$, molar <1, nor peralkaline field]. Profuse crystallization of calcic plagioclase + orthopyroxene during low-pressure (≤ 4 kbar) incongruent melting explains all of the major and trace element characteristics of A-type granites (e.g., their low Al, Ca, Mg, Sr, and Eu contents, and high Ga/Al ratios). Patiño Douce (1997) concluded that the shallow origin of A-type granites is in turn a consequence of their genesis in extensional, or at least non-compressive, tectonic regimes, where the crust tends to be thin and magmatic advection of heat can approach the Earth's surface. The A-type chemical characteristics are therefore lost in the deep crust, explaining the absence of A-type magmas from compressive tectonic environments where the crust is thick. Dahlquist et al. (2010) have suggested that the Early Carboniferous metaluminous A-type granites of the Eastern Sierras Pampeanas (Early Gondwana magmatism) were emplaced in an extensional intraplate setting and a non-compressive tectonic regime rather than the syn-kinematic emplacement invoked for the Devonian granites of Córdoba and San Luis by Sims et al. (1998) and López de Luchi et al. (2004, 2007). Dahlquist et al. (2006) and Grosse et al. (2009) studied Carboniferous granites in the Sierra de Velasco (Fig. 1) emphasizing their nearly circular shape and the absence of pervasive deformation, which would suggest an extensional regime during the emplacement of the plutons and Late Carboniferous mafic dykes dated at 309 and 311 Ma in the granites of the Achala batholith and the Los Árboles pluton (Caprano et al. 2012; Dahlquist and Alasino 2012). However, a full understanding of the emplacement of the Capilla del Monte pluton would require structural studies such as those carried out on the Mid-Devonian granites of the Sierra de San Luis (e.g., Siegesmund et al. 2004; López de Luchi et al. 2007).

Based on geochemical and isotopic data, Alasino et al. (2012) concluded that the Early Carboniferous A-type magmatism of Sierras Pampeanas was generated in a retro-arc setting with a progressive lithospheric thinning toward the west, leading to participation of more juvenile material in the magmas.

Recent new geochemical and geochronological data (Dahlquist et al. 2014a, 2015) support the presence of a magmatic arc from the Early Carboniferous, located in the western margin of Gondwana (i.e., present-day Cordillera Frontal and Western Sierras Pampeanas) with the synchronous development of A-type magmatism in the margin region (now the Eastern Sierras Pampeanas). Therefore, any geodynamic setting for Carboniferous time must include the presence of both a magmatic arc and within-plate magmatism.

Petrological, geochemical, and isotopical data

Both the Achala batholith and Capilla del Monte pluton have dominant and mostly restricted monzogranite composition and similar major element content (Fig. 3a, b), with peraluminous ASI values (see Table 1; Dahlquist et al. 2014b). This distinguishes the Capilla del Monte pluton from the Early Carboniferous granites of Eastern Sierras Pampeanas farther to the west, which have dominantly metaluminous composition (see Dahlquist et al. 2010; Alasino et al. 2012). The Capilla del Monte pluton is a two-mica granite, whereas biotite is dominant in the other A-type granites of the Eastern Sierras Pampeanas, and the Cerro La Gloria pluton, the westernmost A-type granite, has magmatic amphibole (edenite).

The granitic facies of the Capilla del Monte pluton have concentrations of high field-strength elements (Y, Nb, Ga, Ta, U, Th, LREE, etc.) comparable to those reported for granitic rocks of Achala batholith. Furthermore, the patterns of REE are similar with pronounced negative Eu anomalies (see Rapela et al. 2008a; Dahlquist et al. 2014b).

A significant feature observed in the Achala batholith, the Carboniferous granites of the Eastern Sierras Pampeanas, and the Capilla del Monte pluton is the concentration of F. As noted above, both the Achala batholith and Capilla del Monte pluton are markedly enriched in Ga and distinct in this respect from the Ordovician calc-alkaline granites of the Famatinian orogen (Fig. 11).

Petrogenetic models for A-type granites commonly invoke igneous source rocks (e.g., Collins et al. 1982; Creaser et al. 1991; Frost and Frost 1997), and peraluminous A-type granites are uncommon. Fayalite granite is a member of the most reduced A-type granites, commonly thought to have been primarily sourced from tholeiitic rocks. Huang et al. (2011) have reported fayalite-bearing A-type granite produced by high-temperature melting of granulitic metasedimentary rocks. Dahlquist et al. (2010) concluded that A-type granites represent variable mixtures of asthenospheric mantle and continental crust, and that different mixtures lead to different (and numerous) subtypes (illustrating

the lack of consensus about A-type magma origin, Bonin 2007). King et al. (1997) suggested that A-type granites in the Lachlan Fold Belt of SW Australia were derived from the partial melting of an infracrustal felsic source, leading to the formation of "aluminous" (metaluminous and weakly peraluminous) A-type granites. Alternatively, the Achala batholith and Capilla del Monte pluton could represent a subtype of A-type granite derived from a crustal source with a dominant metasedimentary component, as indicated by their whole-rock chemistry (high ASI values), mineralogy (biotite and muscovite), and the Sr and Nd isotope data. In fact, the Achala batholith has been considered as a F-rich peraluminous A-type granite derived from a continental source (Rapela et al. 2008a; Dahlquist et al. 2013, 2014b).

Thus, although present geochronological data distinguish two magmatic events (i.e., Late Devonian for the Achala batholith and Early Carboniferous for the Capilla del Monte pluton, with a time difference of about 30 Ma), petrological and geochemical characteristics show that both granites represent F-rich peraluminous A-type magmatism.

Hf isotope data in zircon for the two igneous bodies are somewhat different: Whereas those for the Capilla del Monte pluton indicate a minor contribution of more juvenile material in the ultimate source, a larger data set for the Achala batholith (Dahlquist et al. 2013, not show here) indicates a more uniformly crustal origin.

The overall petrological and geochemical similarities between the Late Devonian Achala batholith and the Early Carboniferous Capilla del Monte pluton suggest the same Mesoproterozoic crustal source and as similar magma-generating setting, but at this stage there is no evidence that they belong to a continuous tectonomagmatic scenario, and their age difference could be taken as arguing against it.

Conclusions

1. The Capilla del Monte pluton was emplaced in Early Carboniferous time, U–Pb and Rb–Sr dating yielding consistent ages of 336 ± 3 and 337 ± 2 Ma (both corresponding to Visean).
2. Capilla del Monte is the easternmost outcrop of the Early Carboniferous magmatism in this part of the pre-Andean margin of Gondwana.
3. Considering previous work and the data reported here, the Capilla del Monte pluton is a F-rich peraluminous intraplate A-type granite, which fits the trend of increasing crustal character toward the east previously established for metaluminous A-type Early Gondwana magmatism in the Sierras Pampeanas.
4. Differentiation of the pluton occurred by fractional crystallization of a uniform parent magma, dominantly of plagioclase and K-feldspar.

5. As well as the dominant continental source material for the Capilla del Monte pluton, a more juvenile component, such as younger metasedimentary rocks or an initially more juvenile magma, also seems to have been involved, as indicated by Hf isotope data in zircon. However, the resultant magma, apart from already crystallized zircon, must have been fully homogenized prior to differentiation of the exposed pluton.
6. The geochronological data collection for granitic rocks of the Sierras de Córdoba allows the distinction of two magmatic events: Late Devonian (Achalian magmatism) and Early Carboniferous (Early Gondwana magmatism). Petrological and geochemical data suggest that geodynamic setting for these episodes was the same (intraplate magmatism), leading to the generation of F-rich peraluminous A-type magmas. However, Hf isotope data suggest an increase in the juvenile material during the Early Carboniferous. New studies are required to understand whether these magmatic events are two independent episodes or may represent a continuous development of the same episode. This would have a significant bearing on the analysis of the deformational history of this area during the Late Devonian to Late Carboniferous interval.

References

Agulleiro Insúa L, Coniglio J, D'Eramo F, Pinotti L, Demartis M, Petrelli H (2013) Plutón Capilla del Monte, Sierras de Córdoba: nuevos aportes metalogénicos, cartográficos y petrológicos. Avances en Mineralogía, Metalogenia y Petrología, pp 275–280

Alasino PH, Dahlquist JA, Pankhurst RJ, Galindo C, Casquet C, Rapela CW, Larrovere M, Fanning CM (2012) Early Carboniferous sub- to mid-alkaline magmatism in the Eastern Sierras Pampeanas. NW Argentina: a record of crustal growth by the incorporation of mantle-derived material in an extensional setting. Gondwana Res 22:992–1008

Anderson JL (1983) Proterozoic anorogenic granite plutonism of North America, In: Medaris LG Jr, Byers CW, Mickelson DM, Shanks WC (eds) Proterozoic geology: selected papers from an international Proterozoic symposium. Geol Soc Am Mem 161:133–154

Astini R, Martina F, Ezpeleta M, Dávila F, Cawood P (2009) Chronology from rifting to foreland basin in the Paganzo Basin (Argentina), and a reapprisal on the "Eo- and Neohercynian" tectonics along Western Gondwana. XII Congreso Geológico Chileno, Santiago, Actas, pp 22–26

Astini RA, Martina F, Dávila FM (2011) The Los Llantenes Formation in the Precordillera of Jagüe (La Rioja Province) and the recognition of a rifting stage in the early evolution of the late Paleozoic basins in western Argentina. Andean Geol 38:245–267

Baldo EG, Verdecchia SO (2014) Las metamorfitas de contacto asociadas al magmatismo Aachaliano de las Sierras de Córdoba. In: del Relatorio XIX (ed) Martino RD, Guereschi A. Congreso Geológico Argentino Geología y Recursos Naturales de la Provincia de, Córdoba, pp 349–363

Baldo EG, Rapela CW, Pankhurst RJ, Galindo C, Casquet C, Verdecchia SO, Murra JA (2014) Geocronología de las Sierras de Córdoba: revisión y comentarios. In: del Relatorio XIX (ed) Martino RD, Guereschi A. Congreso Geológico Argentino, Geología y Recursos Naturales de la Provincia de Córdoba, pp 845–868

Basei MAS, da Costa Campos Neto M, Pacheco Lopes A, Nutman AP, Liu D, Sato K (2013) Polycyclic evolution of Camboriú Complex migmatites, Santa Catarina, Southern Brazil: integrated Hf isotopic and U-Pbage zircon evidence of episodic reworking of a Mesoarchean juvenile crust. Braz J Geol 43:427–443

Bellone D, Murra J (2014) Cartografía y petrología del basamento ígneo-metamórfico del norte de la sierra del Cuniputo, provincia de Córdoba. 19° Congreso Geológico Argentino. Actas: T8-03

Bense F, Wemmer K, Löbens S, Siegesmund S (2014) Fault gouge analyses: K–Ar illite dating, clay mineralogy and tectonic significance—a study from the Sierras Pampeanas. Argent Int J Earth Sci 103:189–218

Blichert-Toft J, Albarede F (1997) The Lu–Hf isotope geochemistry of chondrites and the evolution of the mantle-crust system. Earth Planet Sci Lett 148:243–258

Bonin B (2007) A-type granites and related rocks: evolution of a concept, problems, and prospects. Lithos 97:1–29

Boynton WV (1984) Geochemistry of the rare earth elements: meteorites studies. In: Henderson P (ed) Rare Earth Element Geochemistry. Elsevier, Amsterdam, pp 63–114

Candiani JC, Stuart-Smith P, Lyons P, Carignano C, Miró R, López H (2001) Hoja Geológica 3166-II. Cruz del Eje, Instituto de Geología y Recursos Minerales, Servicio Geológico Minero Argentino, Boletín **249**

Caprano J, Colombo F, Baldo EG, Wemmer K (2012) Basic Magmatism in Eastern Sierras Pampeanas (Córdoba, Argentina): the magmatic record of Late Carboniferous extension. 8° Congreso Geológico de España. Oviedo. Geotemas 13:1912–1914

Casquet C, Rapela CW, Pankhurst RJ, Baldo EG, Galindo C, Fanning CM, Dahlquist J (2012) Fast sediment underplating and essentially coeval juvenile arc magmatism in the Ordovician continental margin of Gondwana, Western Sierras Pampeanas, Argentina. Gondwana Res 22:664–673

Cerný P, Meintzer RE, Anderson AJ (1985) Extreme fractionationion rare element granitic pegmatites: selected examples of data and mechanisms. Can Miner 23:381–421

Chappell BW, White AJR (1992) I- and S-type granites in the Lachlan fold belt. Trans R Soc Edinb Earth Sci 83:1–26

Collins WJ (2002) Hot orogens, tectonic switching, and creation of continental crust. Geology 30:535–538

Collins WJ, Beams SD, White AJR, Chappell BW (1982) Nature and origin of A-type granites with particular reference to southeastern Australia. Contrib Miner Petrol 80:189–200

Creaser RA, Price RC, Wormald RJ (1991) A-type granites revisited: assessment of a residual-source model. Geology 19:163–166

Dahlquist JA, Alasino PH (2012) Primera edad U–Pb en circón usando LA-ICP-MS de un dique traquiandesítico emplazado en el granito tipo-A Los Árboles, Sierras Pampeanas Orientales. Revista de la Asoc Geol Arg 69:294–297

Dahlquist JA, Rapela CW, Pankhurst RJ, Baldo E, Saavedra J, Alasino PH (2005) Los granitoides de la sierra de Chepes y su comparación con granitoides paleozoicos de las Sierras Pampeanas: implicancias para el orógeno famatiniano. In: Dahlquist JA, Baldo EG, Alasino PH (eds) Geología de la provincia de La Rioja—Precámbrico–Paleozoico Inferior, Asociación Geológica Argentina, Serie D, Publicación Especial No. 8, pp 87–108

Dahlquist JA, Pankhurst RJ, Rapela CW, Casquet C, Fanning CM, Alasino P, Baez FM (2006) The San Blas Pluton: an example of Carboniferous plutonism in the Sierras Pampeanas, Argentina. J S Am Earth Sci 2:341–350

Dahlquist JA, Pankhurst RJ, Rapela CW, Galindo C, Alasino P, Fanning CM, Saavedra J, Baldo E (2008) New SHRIMP U–Pb data from the Famatina complex: constraining Early-Mid Ordovician Famatinian magmatism in the Sierras Pampeanas, Argentina. Geol Acta 6:319–333

Dahlquist JA, Alasino PH, Eby GN, Galindo C, Casquet C (2010) Fault controlled Carboniferous A-type magmatism in the proto-Andean foreland (Sierras Pampeanas, Argentina): geochemical constraints and petrogenesis. Lithos 115:65–81

Dahlquist JA, Pankhurst RJ, Gaschnig RM, Rapela CW, Casquet C, Alasino PH, Galindo C, Baldo E (2013) Hf and Nd isotopes in Early Ordovician to Early Carboniferous granites as monitors of crustal growth in the Proto-Andean margin of Gondwana. Gondwana Res 23:1617–1630

Dahlquist JA, Basei M, Alasino PH, Campos M, Casquet C (2014a) The geological setting of Carboniferous magmatism in the proto-Andean margin of Gondwana, Sierra Pampeanas, Argentina. In: Pankhurst RJ, Castiñeiras P, Sánchez Martínez S (eds) Gondwana 15—North meets South, Abstracts Book, Instituto Geológico y Minero de España, Madrid, Spain, p 46

Dahlquist JA, Alasino PH, Bello C (2014b) Devonian F-rich peraluminous A-type magmatism in the proto-Andean foreland (Sierras Pampeanas, Argentina): geochemical constraints and petrogenesis from the western-central region of the Achala batholith. Miner Petrol 108:391–417

Dahlquist JA, Morales Cámera MM, Alasino PH (2015) Petrografía, química mineral y geoquímica comparada de los plutones Potrerillos y Cerro La Gloria: magmatismo de arco y retroarco en el carbonífero inferior. Revista de la Asoc Geol Arg 72(2):167–181

de La Roche H (1992) Un homologue cationique du triangle Q–A–P (quartz–feldspath alcalin–plagioclase), figure majeure de la pétrologie des roches plutoniques. Comptes Rendus de l'Académie des Sciences, París, Série II 315:1687–1693

DePaolo DJ, Linn AM, Schubert G (1991) The continental crustal age distribution; methods of determining mantle separation ages from Sm–Nd isotopic data and application to the Southwestern United States. J Geophys Res B96:2071–2088

Domeier M, Torsvik TH (2014) Plate tectonics in the late Paleozoic. Geosci Front 5:303–350

Dorais M, Lira R, Chen Y, Tingey D (1997) Origin of biotite–apatite-rich enclaves, Achala Batholith, Argentina. Contrib Miner Petrol 130:31–46

Ducea MN, Otamendi JE, Bergantz G, Stair KM, Valencia VA, Gehrels GE (2010) Timing constraints on building an intermediate plutonic arc crustal section: U–Pb zircon geochronology of the Sierra Valle Fértil–La Huerta, Famatinian arc, Argentina. Tectonics 29(TC4002):21–22

Eby GN (1992) Chemical subdivision of the A-type granitoids: petrogenetic and tectonic implications. Geology 20:641–644

Ewart A, Griffin WL (1994) Application of proton-microprobe data to trace-element partitioning in volcanic-rocks. Chem Geol 117:251–284

Franchini M, Lira R, Meinert L, Ríos FJ, Poklepovic MF, Impiccini A, Millone H (2005) Na–Fe–Ca Alteration and LREE (Th–Nb).

Mineralization in marble and granitoids of Sierra de Sumampa, Santiago del Estero, Argentina. Econ Geol 100:733–764

Frost CD, Frost BR (1997) Reduced rapakivi-type granites: the tholeiite connection. Geology 25:647–650

Frost BR, Barnes CG, Collins WJ, Arculus RJ, Ellis DJ, Frost CD (2001) A geochemical classification for granitic rocks. J Petrol 42:2033–2048

García MG, Lecomte KL, Stupar Y, Formica SM, Barrionuevo M, Vesco M, Gallará R, Ponce R (2012) Geochemistry and health aspects of F-rich mountainous streams and groundwaters from Sierras Pampeanas de Cordoba, Argentina. Environ Earth Sci 65:535–545

Goodge JW, Vervoort JD (2006) Origin of mesoproterozoic A-type granites in Laurentia: Hf isotope evidence. Earth Planet Sci Lett 243:711–731

Gregori DA, Fernández-Turiel JL, López-Soler A, Petford N (1996) Geochemistry of upper palaeozoic-lower triassic granitoids of the central frontal cordillera (33°10′–33°45′), Argentina. J South Am Earth Sci 9:141–151

Grosse P, Söllner F, BaézMA Toselli AJ, Rossi JN, de la Rosa JD (2009) Lower carboniferous post-orogenic granites in central-eastern Sierra de Velasco, Sierras Pampeanas, Argentina: U–Pb monazite geochronology and Sr–Nd isotopes. Int J Earth Sci 98:1001–1025

Höckenreiner M, Söllner F, Miller H (2003) Dating the TIPA shear zone: an early Devonian terrane boundary between the Famatinian and Pampean systems (NW Argentina). J S Am Earth Sci 16:45–66

Huang HQ, Li XH, Li WX, Li ZX (2011) Formation of high δ18O fayalite-bearing A-type granite by high-temperature melting of granulitic metasedimentary rocks, southern China. Geology 39:903–906

Icenhower JP, London D (1996) Experimental partitioning of Rb, Cs, Sr, and Ba between alkali feldspar and peraluminous melt. Am Mineral 81:719–734

Johnson DM, Hooper PR, Conrey RM (1999) XRF analysis of rocks and minerals for major and trace elements on a single low dilution Litetraborate fused bead. Adv X-ray Anal 41:843–867

Kemp AIS, Hawkesworth CJ, Foster GL, Paterson GA, Woodhead JD, Hergt JM, Gray CM, Whitehouse MJ (2007) Magmatic and crustal differentiation history of granitic rocks from Hf–O isotopes in zircon. Science 315:980–983

King PL, White AJR, Chappell BW, Allen CM (1997) Characterization and origin of aluminous A-type granites from the Lachlan Fold Belt, southeastern Australia. J Petrol 38:371–391

Konopelko D, Biske G, Seltmann R, Eklund O, Belyatsky B (2007) Hercynian postcollisional A-type granites of the Kokshaal Range, Southern Tien Shan, Kyrgyzstan. Lithos 97:140–160

Limarino C, Tripaldi A, Marenssi S, Fauqué L (2006) Tectonic, sea-level, and climatic controls on Late Paleozoic sedimentation in the western basins of Argentina J S Am. Earth Sci 22:205–226

Linares E (1966) Datación geológica de las rocas graníticas de las Sierra de Córdoba por medio del método plomo-alfa (Larsen). Actas 3er Jornadas Geológicas Argentinas Comodoro Rivadavia, Actas 2:199–206

Linares E, Latorre CO (1969) Edades potasio-argón y plomo-alfa de rocas graníticas de las provincia de Córdoba y de San Luis. 6 Jornadas Geológicas Argentinas Mendoza, Actas 2:195–204

Llambías EJ, Sato AM (1995) El batolito de Colangüil: transición entre orogénesis y anorogénesis. Revista de la Asoc Geol Arg 50:111–131

López de Luchi MG, Rapalini AE, Siegesmund S, Steenken A (2004) Application of magnetic fabrics to the emplacement and tectonic history of Devonian granitoids in central Argentina. In: Martín-Hernández F, Lüneburg CM, Aubourg C, Jackson M

(eds). Magnetic fabric: methods and applications. Geological Society, London, Special Publications 238:447–474

López de Luchi M, Siegesmund S, Wemmer K, Steenken A, Naumann R (2007) Geochemical constraints on the petrogenesis of the Paleozoic granitoids of the Sierra de San Luis, Sierras Pampeanas, Argentina. J S Am Earth Sci 24:138–166

Ludwig KR (2003) Isoplot/ex version 3.0: a geochronological toolkit for Microsoft Excel. Berkeley Geochronology Center Special Publication No. 4, 2455 Ridge Road, Berkeley CA 94709, USA

Lyons P, Skirrow RG, Stuart-Smith PG (1997) Geology and Metallogeny of the Sierras Septentrionales de Córdoba. 1:250.000 Map Sheet, Province of Córdoba. Geoscientific mapping of the Sierras Pampeanas. Argentine—Australia Cooperative Project. Anales del Servicio Geológico Minero Argentino, Buenos Aires 27:1–131

Malvin DJ, Drake MJ (1987) Experimental determination of crystal/melt partitioning of Ga and Ge in the system forsterite–anorthite–diopside. Geochim Cosmochim Acta 51:2117–2128

Martino R, Kraemer P, Escayola M, Giambastiani M, Arnosio M (1995) Transecta de las Sierras Pampeanas de Córdoba a los 32°S. Revista de la Asoc Geol Arg 50:60–77

Massabie C (1982) Geología de los alrededores de Capilla del Monte y San Marcos. Provincia de Córdoba. Revista de la Asoc Geol Arg 37:153–173

Miller CF, McDowell SM, Mapes RW (2003) Hot and cold granites? Implications of zircon saturation temperatures and preservation of inheritance. Geology 31:529–532

Murra J, Baldo E (1996) El Granito de Capilla del Monte y su encajónate ígneo-metamórfico, Sierras Pampeanas de Córdoba. XIII, Congreso Geológico Argentino y II Congreso de Exploración de Hidrocarburos. Actas III:499–505

Nakamura N (1974) Determination of REE, Ba, Mg, Na and K in carbonaceous and ordinary chondrites. Geochim Cosmochim Acta 38:757–773

Nash WP, Crecraft HR (1985) Partition coefficients for trace elements in silicic magmas. Geochim Cosmochim Acta 49:2309–2322

Pankhurst RJ, O'Nions RK (1973) Determination of Rb/Sr and $^{87}Sr/^{86}Sr$ ratios of some standard rocks and evaluation of X-ray fluorescence spectrometry in Rb-Sr geochemistry. Chem Geol 12:127–136

Pankhurst RJ, Rapela CW, Saavedra J, Baldo E, Dahlquist J, Pascua I, Fanning CM (1998) The Famatinian magmatic arc in the southern Sierras Pampeanas. In: Pankhurst RJ, Rapela CW (eds) The Proto-Andean Margin of Gondwana. Special Publication of the Geological Society, London No. 142, 343–367

Pankhurst RJ, Rapela CW, Fanning CM (2000) Age and origin of coeval TTG, I- and S-type granites in the Famatinian belt of NW Argentina. Trans R Soc Edinb Earth Sci 91:151–168

Patiño Douce AE (1997) Generation of metaluminous A-type granites by low-pressure melting of calc-alkaline granitoids. Geology 25:743–746

Patiño MLG, Patiño Douce AE (1987) Petrología y petrogénesis del batolito de Achala, provincia de Córdoba, a la luz de la evidencia de campo, Revista de la Asoc Geol Arg 42:201–205

Pinotti L, Coniglio JE, Esparza AM, D'Eramo F, Llambías EJ (2002) Nearly circular plutons emplaced by stoping at shallow crustal levels, Cerro Aspero batholith, Sierras Pampeanas de Córdoba, Argentina. J S Am Earth Sci 15:251–265

Rapela CW, Llambías EJ (1999) El magmatismo Gondwánico y los ciclos fanerozoicos. In: Caminos R (ed) Geología Argentina. Servicio Geológico Minero Argentino, Buenos Aires, pp 364–372

Rapela CW, Pankhurst RJ, Kirschbaum A, Baldo EGA (1991) Facies intrusivas de edad carbonífera en el batolito de Achala: ¿Evidencia de una anatexis regional en las Sierras Pampeanas? 6

Congreso Geológico Chileno Viña del Mar, Chile, Extended Abstracts 1:40–43

Rapela CW, Pankhurst RJ, Casquet C, Baldo E, Saavedra J, Galindo C, Fanning CM (1998) The Pampean orogeny of the southern proto-Andes: Cambrian continental collision in the Sierras de Córdoba. In: Pankhurst, RJ and Rapela, CW (eds) The Proto-Andean Margin of Gondwana. Geol Soc Lond Spec Publ 142:181–217

Rapela CW, Pankhurst RJ, Casquet C, Fanning CM, Baldo EG, González-Casado JM, Galindo C, Dahquist J (2007) The Río de la Plata craton and the assembly of SW Gondwana. Earth Sci Rev 83:49–82

Rapela CW, Baldo EG, Pankhurst RJ, Fanning CM (2008a) The Devonian Achala batholith in the Sierras Pampeanas: F-rich aluminous A-type granites. In: VI South American symposium on isotope geology, San Carlos de Bariloche, Argentina, Proceedings in CD-ROM, paper 53

Rapela CW, Pankhurst RJ, Dahquist J, Baldo EG, Casquet C, Galindo C (2008b) Revisiting accretionary history and magma sources in the Southern Andes: Time variation of "typical Andean granites". In: International symposium on Andean geodynamics (ISAG 2008, Nice), extended abstracts: 427–430

Rittmann A (1957) On the serial character of igneous rocks. Egypt J Geol 1:23–48

Sato K, Siga O Jr, Silva JA, McReath I, Liu D, Iizuka T, Rino S, Hirata T, Sproesser WM, Basei MAS (2009) In situ isotopic analyses of U and Pb in zircon by remotely operated SHRIMP II, and Hf by LA-ICP-MS: an example of dating and genetic evolution of zircon by ^{176}Hf/^{177}Hf from the Ita Quarry in the Atuba Complex, SE Brazil. Geologia Universidade São Paulo, Série Científica São Paulo 9:61–69

Sato K, Basei MAS, Ferreira CM, Vlach SRF, Ivanuch W, Siga O Jr, Onoi AT (2010) In situ U–Th–Pb isotopic analyses by Excimer laser ablation/ICP–MS on Brazilian xenotime megacrystal: first U–Pb results at CPGeo-IG-USP. VII South American Symposium on Isotope Geology, Brasília, DF, CD Rom

Sato K, Basei MAS, Ferreira CM, Sproesser WM, Vlach SRF, Ivanuch W, Onoi AT (2011) U–Th–Pb analyses by excimer laser ablation/ICP–MS on MG Brazilian xenotime. Goldschmidt—2011. Miner Mag 1801

Scherer E, Whitehouse MJ, Münker C (2007) Zircon as a monitor of crustal growth. Elements 3:19–24

Schwartz JJ, Gromet LP, Miro R (2008) Timing and duration of the calcalkaline arc of the Pampean orogeny: implications for the late Neoproterozoic to Cambrian evolution of Western Gondwana. J Geol 116:39–61

Shand SJ (1927) The eruptive rocks. John Wiley, New York **360 pp**

Siegesmund S, Steenken A, López de Luchi MG, Wemmer K, Hoffmann A, Mosch S (2004) The Las Chacras-Potrerillos batholith (Pampean Ranges, Argentina): structural evidence, emplacement and timing of the intrusion. Int J Earth Sci 93:23–43

Sims JP, Ireland TR, Camacho A, Lyons P, Pieters PE, Skirrow RG, Stuart-Smith PG, (1998) U–Pb, Th–Pb and Ar–Ar geochronology from the southern Sierras Pampeanas, Argentina: implications for the Palaeozoic tectonic evolution of the western

Gondwana margin. In: Pankhurst RJ, Rapela CW (eds) The Proto-Andean Margin of Gondwana. Geol Soc Lond Spec Publ 142:259–281

Söderlund U, Patchett JP, Vervoort JD, Isachsen CE (2004) The ^{176}Lu decay constant determined by Lu–Hf and U–Pb isotope systematics of Precambrian mafic intrusions. Earth Planet Sci Lett 219:311–324

Streck MJ, Grunder AL (1997) Compositional gradients and gaps in high-silica rhyolites of the Rattlesnake Tuff, Oregon. J Petrol 38:133–163

Streckeisen A (1976) To each plutonic rock its proper name. Earth Sci Rev 12:1–33

Stuart-Smith PG, Camacho A, Sims JP, Skirrow RG, Pieters PE, Black LP, Miró R (1999) Uranium–lead dating of felsic magmatic cycles in the southern Sierras Pampeanas, Argentina: implications for the tectonic development of the proto-Andean Gondwana margin. Laurentia Gondwana connections before Pangea: In: Ramos VA, Keppe ID (eds) Geol Soc Am Spec Paper 33:87–114

Sun SS, McDonough WF (1989) Chemical and isotopic systematics of oceanic basalts; implications for mantle composition and processes. Magmatism in the ocean basins: In: Saunders AD, Norry MJ (eds) Geol Soc Lond Spec Publ 42:313–345

Vervoort JD, Blichert-Toft J (1999) Evolution of the depleted mantle: Hf isotope evidence from juvenile rocks through time. Geochim Cosmochim Acta 63:533–556

Villaros A, Buick IS, Stevens G (2012) Isotopic variations in S-type granites: an inheritance from a heterogeneous source? Contrib Miner Petrol 163:243–257

Watson EB, Harrison TM (1983) Zircon saturation revisited: temperature and composition effects in a variety of crustal magma types. Earth Planet Sci Lett 64:295–304

Wemmer KW, Steenken A, Müller S, López de Luchi M, Siegesmund S (2011) The tectonic significance of K/Ar illite fine-fraction ages from the San Luis Formation (Eastern Sierras Pampeanas, Argentina) Int J. Earth Sci 100:659–669

Whalen JB, Currie KL, Chappell BW (1987) A-type granites: geochemical characteristics, discrimination and petrogenesis. Contrib Miner Petrol 95:407–419

Whitmeyer SJ (2008) Dating fault fabrics using modern techniques of ^{40}Ar/^{39}Ar thermochronology: evidence for Paleozoic deformation in the Eastern Sierras Pampeanas, Argentina. In: De Paor D (ed) J Virtual Explor, vol 30, paper 3, doi:10.3809/jvirtex.2008.00207

Whitney DL, Evans BW (2010) Abbreviations for names of rock-forming minerals. Am Mineral 95:185–187

Willner AP, Gerdes A, Massonne H-J, Schmidt A, Sudo M, Thomson SN, Vujovich G (2011) The geodynamics of collision of a microplate (Chilenia) in Devonian times deduced by the pressure–temperature–time evolution within part of a collisional belt (Guarguaraz Complex, W-Argentina). Contrib Miner Petrol 162:303–327

Wilson M (1989) Igneous petrogenesis, a global tectonic approach. Springer, Netherlands. doi:10.1007/978-1-4020-6788-4